

ACTIVATED CARBON FIBERS - PAST, PRESENT, AND FUTURE

by

J. Economy, M. Daley, C. Mangun
1304 West Green Street
Materials Science and Engineering
University of Illinois
Urbana, IL 61801

Introduction

In this paper the background to the development of activated carbon fibers (ACFs) is reviewed, and then some of the recent progress of the past several years is discussed. Finally, a glimpse of the future for this field is provided which builds on some very recent results produced in our group.

The ACFs were first developed in the period of 1969-72 and made available in developmental quantities at that time. Since then, Nippon Kynol, the current manufacturer, has developed a number of niche markets which today have resulted in a multi-million dollar industry. Surprisingly, it is only in the last several years that a number of researchers have begun to examine this very interesting family of materials as witness the number of papers on ACFs in this Symposium.

It should be noted that the ACFs are currently priced in the range of \$100/lb and hence hardly compete with the activated carbon granules (ACGs) which are available for \$1.00/lb. and less. Hence, the ACFs only find commercial application in those areas where the unique textile forms of the ACFs permit use based on the greatly improved contact efficiency of the fibers. For the future, we have recently shown that we can prepare ACFs at a cost much closer to that of ACGs. Hence, one would anticipate a major market opportunity not only as a replacement of ACGs, but also from the creation of many new markets which are not available to ACGs because of the need for containment.

Past (1963 - 1975)

In 1963, at the Carborundum Co. we first showed that we could prepare crosslinked phenolic (phenol formaldehyde) fibers by spinning from a Novolac melt and then curing with $\text{HCl} + \text{CH}_2\text{O}$.⁽¹⁾ This fiber could be processed into a wide range of textile forms by conventional methods. It also displayed an outstanding flame resistance. In 1969 we commercialized this fiber under the trade name Kynol as a potentially low cost textile for use in highly aggressive environments.

More pertinent to this article, we showed in 1968 that we could produce a range of high surface area ACFs by heating the Kynol in steam 700 - 900°C (See Figure 1).⁽²⁾ By 1971 we began to make developmental quantities available commercially in the USA and also a joint venture company in Japan, Nippon Kynol Inc. In 1974, commercial development was transferred to Nippon Kynol and the program was terminated at the Carborundum Company.

During the period of 1968 - 74, we made considerable progress in developing and characterizing the ACFs. Thus, we were able to finalize on three ACFs with nominal surface areas of 1500, 2000 and 2500m²/g. The 2500m²/g ACF was shown to have the highest capacity, but was also the

most brittle. Considerable work was carried out to determine possible advantages over ACGs. It was found that for similar surface areas the ACFs displayed an almost 2x increase in breakthrough times over ACGs for removal of phenol or butane.⁽³⁾ The ACFs could be reactivated in situ by electrical resistance heating at 100 - 200°C (See Table 1). It was also shown that the modestly acidic pore surface of the ACFs could be converted to a basic surface by heating in ammonia at 600 - 900°C.⁽⁴⁾ Finally, it was found that high surface fibers (600m²/g) could be obtained by etching at much lower temperatures of 450°C to produce an activated phenolic fiber (APF).⁽⁴⁾ These fibers appeared to have a smaller pore size distribution, but could be made at somewhat lower cost than the ACFs.

Present (1990 - 94)

Starting in about 1990 we initiated a program at the University of Illinois to develop a far better understanding of the nature of activated carbons. Our intent was that we would not only develop a more predictive capability concerning the adsorption characteristics of ACFs, but that this could also lead to design of much lower cost fiber based systems that would be cost competitive to ACGs. Our expectation was that with a greatly improved understanding of the kinetics of adsorption and of contact efficiencies we would be able to design low cost systems that would be capable of removing trace contaminants in the low parts per billion (ppb) range.

Initially our efforts focused on pursuing possible leads from the work of the early 1970's. Thus we found that we could chemically convert the pore surface of the ACFs to a much wider range of chemistries (See Figure 2).⁽⁵⁾ As a result of these studies it became apparent that we could tailor the pore surface chemistry to be much more acidic or basic or more polar or relatively neutral. Several papers have already been published showing the utility of chemically tailored surfaces for selective removal of VOCs⁽⁶⁾ and of H₂O.⁽⁷⁾ The role of surface area and pore size and shape has also been examined in far greater depth particularly with respect to the dramatic changes in separation of contaminants at high versus low concentrations.⁽⁸⁾ A critical component of this study has been our ability to directly access the porosity in ACFs using Scanning Tunneling Microscopy (STM).⁽⁹⁾ As a result of these studies we are now able to directly measure the microporosity dimensions and correlate these measurements with the adsorption characteristics of the ACFs. All of these issues are discussed in far greater detail in the ensuing paper by Daley, et. al.

The earlier work on the APFs has also been reexamined during the last several years and the conditions for reproducible manufacture have been identified. (See Figure 3) We have also shown that the APFs have modestly improved wear resistance over the ACFs.⁽⁴⁾ As might be expected the microporosity is smaller (in the range of 5 - 7Å as compared to 10 - 13Å for ACF 1500). The potential for design of molecular sieve-like carbon is clearly a possibility from this work.

Future (1996 -)

One of the most exciting aspects of our program has been the recent announcement that we had developed a low cost alternative to ACFs.⁽¹⁰⁾

This was accomplished by coating glass fibers with a phenolic resin. Activation of the phenolic coating can be carried out by any one of a number of techniques normally used for ACFs. Thus, for the first time one has access to a very low cost activated fiber assembly. Typically, phenolic resins are available for 60 - 70¢/lb while the glass fiber, depending on its product form, can cost well under a dollar for non-wovens and somewhat higher for woven textiles. In order to maintain flexibility of the final textile we limit the percentage of phenolic resin to ~30% by volume in the case of woven textiles. With non-woven textiles, paper or felt we can go to much higher loadings of phenolic resin. This may appear to be a limitation in terms of the amount of activated material for a given volume. However, we find that the contact efficiency is greatly improved compared to ACFs which of course are significantly better than ACGs (See Figure 4). Obviously reactivation of the spent assembly would be much faster than with ACFs. From preliminary tests the glass fibers coated with activated carbon can be reactivated by electrical resistance heating at 100 - 200°C or by use of steam at 120 - 170°C.

An important advantage of the activated, glass coated textile is the greatly improved wear resistance of this material. We believe that this arises from the fact that the coating provides protection to the glass fiber surface, which otherwise would be very sensitive to damage.

As a result of our recent announcement concerning this development we have had a number of inquiries from industry concerning commercial availability and utility. Currently, we have identified a number of companies that would be interested in participating in those aspects of the manufacture of this new product where they have a core competency. We are also starting to talk to companies that would be interested in acting as product form assemblers. In the new environment in industry, which requires focusing on one's core business, few companies appear willing to embrace the entire spectrum of activities required for commercial development of a new product. On the other hand, this product appears to lend itself to the establishment of a virtual business involving 3-4 companies to manufacture the product. With such an approach, only a minimal investment in manufacturing and scale-up would be required. A similar argument can be made for product assembly.

One area that we are examining carefully is that of chemical warfare including nerve gases. Up to now, gas masks that depend on ACGs have been in use for the past 50 years. However they are cumbersome and expensive and because of the acidic nature of the pore surface are not as effective against most of the toxic agents which are also acidic. It would seem that fabric which is easily deployed as a hood over the head and shoulders would provide very low cost protection against most all of the chemical warfare agents. To further enhance the adsorption capacity it would be important to activate in such a way that the pores are basic and would bind the toxic chemicals more tightly. If indeed all this proves to be correct, we may have available for the first time the ultimate defense against chemical warfare and one that would discourage future use of such methods by terrorists.

Other directions that we are now beginning to pursue is the use of these new activated assemblies as catalyst supports. We also plan to revisit some of our earlier work of 28 years ago on hyperfilters based on activated membranes⁽¹¹⁾ and on ion exchange fibers⁽¹²⁾ which are tailored to remove specific metal contaminants.

References

1. Economy, J., Flame-Retardant Polymeric Materials, Vol. 2, 1978, Plenum Publishing Corporation, p. 203-226.
2. Lin, R.Y., Economy, J., Applied Polymer Symposium, 1973, 21, p. 143-152.
3. Economy, J., Lin, R. Y., Applied Polymer Symposium, 1976, 29, p. 199.
4. Andreopoulos, A. G., Economy, J., Chemistry of Materials, 1991, Vol. 3, No. 4, p 594.
5. Economy, J., Foster, K. L., Andreopoulos, A. G., Jung, H., ChemTech, October 1992, p. 597.
6. Dimotakis, E. D., Cal, M. P., Economy, J., Rood, M.J., Larson, S. M., Environmental Science and Technology, 1995, Vol. 2, Issue 7.
7. Dimotakis, E. D., Cal, M. P., Economy, J., Rood, M.J., Larson, S. M., Chemistry of Materials (in press).
8. Foster, K. L., Fuerman, R. G., Economy, J., Larson, S. M., Rood, M. J., Chemistry of Materials, 1992, Vol. 4, No. 5, p. 1068.
9. Economy, J., Daley, M., Hippo, E. J., Tandon, D., Carbon, 33, 1995, No. 3, p. 344-345.
10. Mangun, C. L., Daley, M. A., Economy, J., 88th Annual Meeting of Air & Waste Management Association, San Antonio, TX, June 18-23, 1995.
11. Economy, J., Lei, G. IR 100 Award, 1975, Carbon Film Hyperfilter.
12. Economy, J., CHEMTECH, 1980, Vol. 10, p. 240.

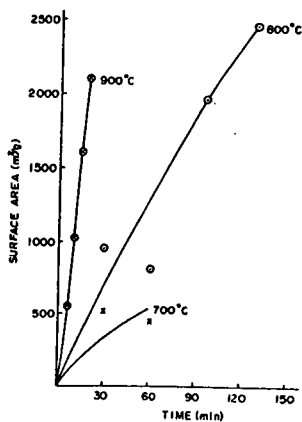


Fig. 1
Steam Activation of Carbonized Kynol Fibers

Sample	PAC Before Adsorption (mg/g)	Reactivation Time (min)	Current (amp)	PAC After Reactivation (mg/g)	Capacity Regain (%)
1	139	10	3	88	66.5
2	140	10	4	—	—
3	153	10	5	46	38.0
4	131	10	2	113	86.0
5	160	10	1	94	58.5

Table 1
Effect of Current Strength on Phenol Adsorption Capacity Regain in Electrical Reactivation

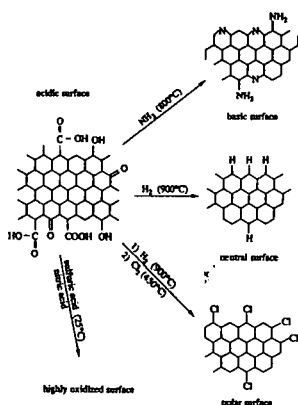


Fig. 2
Chemical Treatment of ACFs Produces a Number of Different Surface Chemistries

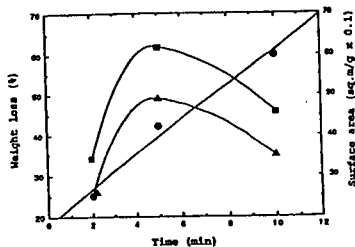


Figure 3
Heating Phenolic on Hot Plate at 450°C for Increasing Times
circle-wt loss (%)
square- Langmuir S.A.
triangle- B.E.T. S.A.

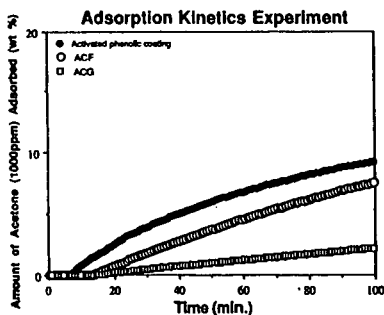


Figure 4
Comparison of Adsorption Kinetics of ACG, ACF, and Activated Phenolic Coating

PREDICTING ADSORPTION PROPERTIES FOR ACFs

M. A. Daley, C. L. Mangun, and J. Economy
1304 West Green Street
Materials Science and Engineering
University of Illinois
Urbana, IL 61801

Keywords: activated carbon fibers (ACFs), pore size, pore surface chemistry

Introduction

Activated carbon fibers (ACFs), and activated carbon granules (ACGs) have been available for about the past 25 and 50 years, respectively. However, selection of the appropriate activated carbon to remove specific contaminants is still very much an empirical process. The problem that exists in creating a more fundamental understanding of these processes is the fact that up to now there has been no direct method for measuring the key parameters. In this paper data are presented which begin to lay the foundations for understanding the adsorption capabilities of ACFs essential to establishing a predictive model.

Factors that Control Adsorption in the Micropore

Many factors control the adsorption in the micropores of the ACFs including the pore size distribution, the pore shape, the pore surface chemistry, the fiber diameter, the adsorbent form, the adsorbate size and shape, the adsorbate chemistry, the physical properties of the adsorbate, the adsorbate concentration, the adsorbate environment, and other adsorbates which may compete for similar sites. In our laboratory, many factors are being examined systematically in great detail. The present status of our work is best summarized by considering the following four questions:

- 1.) How do pores initially form in the ACFs?
- 2.) What is the structure of high surface area ACFs?
- 3.) What is the role of pore size in adsorption?
- 4.) What is the role of pore surface chemistry in adsorption?

How do Pores Initially Form in the ACFs?

The origin of pore formation has recently been elucidated for ACFs (1). This discovery came about when it was observed that high surface area carbon fibers were produced during activation of phenolic fiber precursors under inert conditions. Presumably, the microporous structure was created by the evolution of volatile by-products at temperatures as low as 400-500°C and its persistence during further heating must be due to the presence of a stable crosslinked structure. Images of this microporous structure were obtained from scanning tunneling microscopy (STM) which provided direct insight into the size and shape of these initial pores. From cross-sectional images of the fiber, a remarkably homogeneous microporous structure was observed in which pores measured from several tenths of nm up to 1.1 nm in diameter with the majority of pores measuring less than 0.6 nm in diameter. At the fiber

surface, the pores were less than 5 nm in diameter and are larger than those in the bulk due to the rapid evolution of volatiles near the carbonization temperature. The initial pores which were observed from STM were not slit-shaped as originally proposed by Dubinin (2) but were ellipsoidally shaped. Thus for the first time an unambiguous interpretation now exists as to the origin of micropores in the ACFs.

What is the Structure of High Surface Area ACFs?

The phenolic fibers can be further activated using an etchant or oxidizing agent. Commercially, the ACFs are activated in a mixture of CO₂ and steam at high temperatures (600 -800 °C) to produce a family of materials with controlled surface area ranging from 700 to 2800 m²/g (3). In practically all cases there is 2-5 % oxygen present in the ACF with a considerable percentage at the pore surface in the form of phenolic and carboxylic units.

The porous structure of the ACFs has been examined at great length using a number of indirect techniques such as fundamental adsorption theory (4), x-ray and neutron scattering (5), and adsorption of different size and shaped molecular probes (6). The greatest progress has been made with STM and we now have a database of over 800 images (7). The initial pores which were formed during carbonization begin to widen when exposed to steam/carbon dioxide due to diffusion of these etchants into the fiber bulk. Throughout activation the pores in the fiber bulk remain homogeneous and average pore sizes measure between 1 and 2 nm depending on the duration of activation (Fig. 1). Again, in contradiction to Dubinin (2), the pores remain ellipsoidally shaped in the bulk of the fiber and do not take on a slit-shaped character. Compared to the homogeneous micropores in the bulk of the fiber, the surface porosity was more heterogeneous and large mesopores and micropores were observed from the extensive reaction at the fiber surface (Fig. 2). A significant decrease in fiber diameter with increasing duration of activation was also noted where the fiber diameter decreases from 15 μ m to 9-12 μ m. The transition between the surface porosity and that in the bulk occurs in a region less than 32 nm and in this region a narrowing of the pores might lead to wedge-shaped pores.

What is the Role of Pore Size in Adsorption

Pore size is one of the most important factors affecting adsorption. In order for adsorption to occur, the adsorbate must fit into the pore. Foster showed a cross-over regime for the adsorption of butane where lower surface area ACFs adsorb better at low concentrations due to a higher overlap in potential which binds the adsorbate more tightly (4). At higher concentrations the higher surface area ACFs adsorbed larger amounts due to a larger pore volume (8). From recent studies, we have observed that the cross-over regime shifts to higher concentrations with lower boiling point adsorbates and to lower concentrations with higher boiling point adsorbates (9). The APFs which have a much smaller pore size in the bulk permit enhanced adsorption of contaminants at ppm levels to ppb levels (Fig. 3). The equilibrium amount adsorbed and its dependence on adsorbate size and boiling point has been related to physical constants using fundamental adsorption theory.

The adsorption kinetics or the rate at which equilibrium adsorption is approached at a given concentration is strictly dependent on the diffusion pathlength. This property is also a function of the adsorbent size and shape, the number and size and shape of pores at the fiber surface and the number and size and shape of pores in the bulk and their

interconnectivity. Our basic studies using ACFs have shown that the rate of adsorption/desorption is faster for materials with larger pores and broader pore size distributions (Fig. 4). The larger pores facilitate fast diffusion to the smaller pores which bind the adsorbate more tightly allowing it to be adsorbed.

Therefore it becomes important to have a good distribution of large and small pores. One reason why the adsorption kinetics of the ACFs is much faster than the granules is because the ACFs have many large mesopores at the fiber surface which permits rapid access to the homogeneous microporous structure in the bulk. ACGs can not usually be tailored in this manner since they contain far fewer pores than the ACFs at their surface and typically they have a much broader pore size distribution in the bulk. One dimension for control of adsorption kinetics in ACGs is the particle diameter. Generally, as the particle diameter decreases the adsorption kinetics increase because the diffusion pathlength decreases.

As the adsorbate size decreases or the concentration decreases, materials with a larger concentration of pore sizes closer to the adsorbate size will have a higher equilibrium adsorption.

Based on these fundamental studies and others it has been possible to design/tailor adsorbents to remove contaminants from air and water to below several ppb level with little increase in estimated cost.

What is the Role of Pore Surface Chemistry in Adsorption

The pore surface chemistry plays an equally critical role in adsorption and can be tailored through chemical activation or through posttreatment. The advantages of chemical activation are that a single step treatment is all that is required to control the surface chemistry and pore size and this can lead to higher reaction yields.

Activation of the phenolic precursors in air results in a high surface area fiber with acidic surface chemistry. When this fiber is activated below the carbonization temperature a unique material is formed which has higher activation yields and better wear properties (10). Under these conditions a family of adsorbents has been developed with as much as 30% oxygen in the form of phenolic hydroxyls. Based on a molecular probe study, these materials have a pore size distribution which is less than 7 Å and may be tailored by controlling the activation conditions. Through control of pore size and acidic surface chemistry, small molecules such as ammonia may be removed to low concentrations (< ppm).

Surprisingly, ammonia will etch the phenolic precursors and may be used to activate them to create high surface area carbon fibers at temperatures as low as 500°C. These materials are basic containing as much as 10 wt% nitrogen usually in the form of pyridine-like groups and aromatic amines depending on the activation conditions. Yields are much higher than that of ACFs that are posttreated in ammonia. Preliminary results have indicated that a large number of acidic contaminants can be selectively removed from air and water.

The ACFs have also been posttreated (8) in chlorine, ammonia, oxidizing agents, or hydrogen to create an ACF with a polar, basic, (basic, polar, or acidic surface chemistry depending on agent used), or neutral surface chemistry, respectively. Depending on the chemistry of the adsorbate, the ACFs can be tailored for selective removal of an adsorbate. For example, ammonia activation of a phenolic precursor permits enhanced adsorption of acidic contaminants such as HCl from air or paranitrophenol from water (Fig. 5). A post-treatment of an ACF with strong acid will produce a number of surface functionalities such as carboxylic acids, phenolic hydroxyls, and quinones. The surface of this material is therefore both acidic and polar thus enhancing the adsorption of both polar (i.e.

acetone) and basic (i.e. ammonia (11)) contaminants (Fig. 6). To date we have developed and characterized approximately 75 different materials with various surface chemistries and pore sizes (12). From these materials we have developed an extensive data base which relates the synthesis conditions to the number and type of functional groups and subsequently relates the effects of these groups to adsorption.

Conclusions/ Future Work

Some of the key parameters important for controlling adsorption have been described in this paper. Selective adsorption of specific adsorbates has been indicated. This work provides the necessary foundation for the next step which is to establish a predictive capability. We are now in the process of relating these material features to the key engineering parameters.

References

1. Economy, J., Daley, M., Hippo, E. J., Tandon, D., *Carbon*, **33**, 3, 344-345 (1995).
2. Dubinin, M. M., Plavnik, G. M., Zaverina, E. D., *Carbon*, **2**, 261-268 (1964). Stoekli, H. F., *Carbon*, **28**, 1, (1990).
3. Lin, R. Y., Economy, J., *Applied Polymer Symposium*, **21**, 143-152, (1973).
4. Foster, K. L., Fuerman, R. G., Economy, J., Larson, S. M., Rood, M. J., *Chemistry of Materials*, **4**, 5, 1068, (1992).
5. Kieffer, J., *J. Appl. Phys.*, **72**, 12, (1992).
6. Kasaoka, S., Sakata, Y., Tanaka, E., Naitoh, R., *International Chemical Engineering*, **29**, 4, 734-742 (October 1989).
7. Daley, M., Tandon, D., Economy, J., Hippo, E., submitted to *Carbon*.
8. Economy, J., Foster, K. L., Andreopolous, A. G., Jung, H., *Chemtech*, **597**, (October 1992).
9. Daley, M., Mangun, C., Economy, J., in preparation.
10. Andreopoulos, A. G., Economy, J., *Chemistry of Materials*, **3**, 4, 594, 1991.
11. Mangun, C., Daley, M., Economy, J., in preparation.
12. Daley, M., Mangun, C., Economy, J., in preparation.

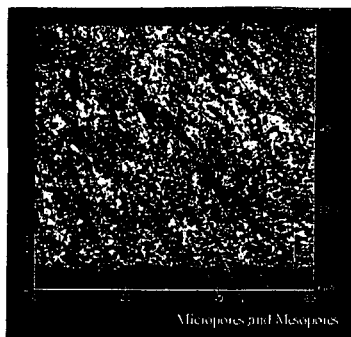


Fig. 1
STM image of the cross-section of an ACF

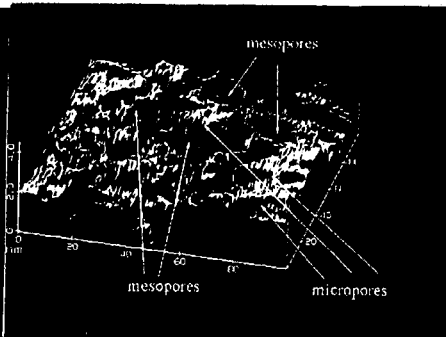


Fig. 2
STM image of the surface of an ACF

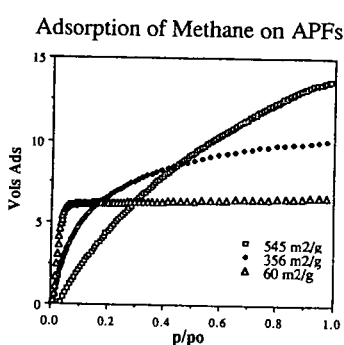


Fig. 3
Lower surface area APFs have smaller average pore sizes which adsorb larger amounts of methane at lower concentrations

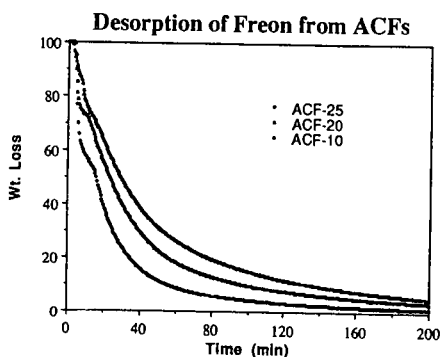


Fig. 4
The larger number ACFs have broader pore size distributions which permits for faster desorption

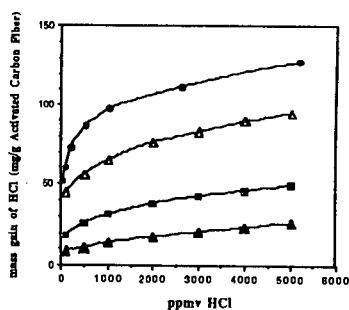


Fig. 5
As the basic character of the ACF increases (wt% N increases), the amount of HCl adsorbed increases proportionally

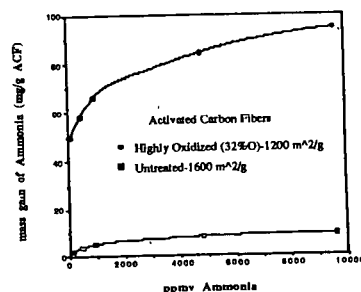


Fig. 6
As the ACF becomes more oxidized, the amount of ammonia adsorbed increases.

HIGH PRESSURE CO₂ ADSORPTION ON ACTIVATED CARBON FIBERS

J. Alcañiz-Monge, D. Cazorla-Amorós and A. Linares-Solano
Dept. Inorganic Chemistry. U. Alicante.
Apt^a 99, Alicante 03080. Spain

Keywords: CO₂ and N₂ adsorptions, High pressures CO₂ adsorption, activated carbon fibers.

INTRODUCTION

Physical adsorption of gases is the most employed technique for the characterization of porous solids [1-3]. N₂ adsorption at 77 K is the more used and, usually, has a special status of recommended adsorptive [4]. The advantage of N₂ adsorption is that it covers relative pressures from 10⁻⁸ to 1, what results in adsorption in the whole range of porosity. The main disadvantage of N₂ adsorption at 77 K is that when used for the characterization of microporous solids, diffusional problems of the molecules inside the narrow porosity (size < 0.7 nm) occur [5].

CO₂ adsorption, either at 273 K or 298 K [5,6], and He adsorption at 4.2 K [7] are two alternatives to N₂ adsorption for the assessment of the narrow microporosity. He adsorption at 4.2 K has been proposed [7] as a promising method for the accurate determination of the microporosity. However, the experimental conditions used (adsorption at 4.2 K) makes this technique not so available as CO₂ adsorption. In the case of CO₂ adsorption the high temperature of adsorption used for CO₂ results in a large kinetic energy of the molecules that can enter into the narrow porosity. In this way, CO₂ adsorption has been proposed as a good complementary technique, not alternative, for the analysis of the porous texture as it could be used to assess the narrow microporosity (size < 0.7 nm).

A confirmation of the reliability of the method for essentially microporous materials, makes necessary the comparison of both N₂ and CO₂ adsorptions at comparable relative pressures where N₂ adsorption has not diffusional limitations. This requires the performance of CO₂ adsorption at high pressures. This type of comparison of both adsorptives has not been performed in the literature through the use of high pressure adsorption experiments.

According to all this, the objectives of this work are the following: i) to cover the lack of studies on CO₂ adsorption at high pressures; ii) to analyze the adsorption of this gas at relative pressures similar to those used with N₂; iii) to show the problems of the use of N₂ adsorption at 77 K specially at low relative pressures. All these objectives can be summarized in confirming of the validity of CO₂ adsorption to characterize microporous carbon materials.

MATERIALS AND METHODS

A series of activated carbon fibers (ACF) obtained from CO₂ (series CFC) activation has been used in this study. The mechanical properties and porosity of these materials have been already analyzed [8]. In summary, the samples are essentially microporous, with a negligible volume of mesopores (only mesoporosity of size larger than 7.5 nm is only observed in samples with high burn-off). Samples with burn-off lower than about 40% have a DR (Dubinin Radushkevich) N₂ volume lower than the DR CO₂ one, what indicates the existence of narrow microporosity where N₂ adsorption has diffusional limitations. The ACF with higher burn-off have some amount of supermicroporosity, as reflected by the larger value of the DR N₂ volume compared to the DR CO₂.

CO₂ adsorption isotherms at 298 K and at high pressures have been carried out in a DMT high pressure microbalance

(Sartorius 4406) connected to a computer for data acquisition. The maximum pressure reached is 4 MPa. Additionally, CO₂ adsorption at 298 K and N₂ adsorption at 77 K up to 0.1 MPa have also been performed with an Autosorb-6 and Omnisorp equipments, respectively, to cover lower relative pressures.

RESULTS AND DISCUSSION

High pressure CO₂ adsorption isotherms at 298 K.

Figure 1 shows CO₂ adsorption isotherms obtained for the samples CFC14 and CFC54, plotted versus the relative fugacity. Each isotherm contains the experiment obtained at sub-atmospheric and at high pressures. It is important to note, by its relevance in the content of the paper, that there is a good continuation in both measurements performed up to sub-atmospheric and high pressures in spite of the different experimental systems used. CO₂ adsorption isotherms can be compared with those obtained from N₂ adsorption at 77 K previously described [8]. The evolution of the isotherms with burn-off is similar for both adsorbates. In fact, several common features can be noted from these experiments: i) the adsorption capacity increases with burn-off and ii) as burn-off increases, the knee of the isotherm widens, showing an increase in microporosity distribution. These results indicate that, due to the range of relative fugacities covered in the high pressure CO₂ adsorption isotherms, this molecule also adsorbs in the supermicroporosity (pore size 0.7-2 nm).

Characteristic curves for N₂ and CO₂ adsorptions.

The characteristic curves that are presented in the following discussion have been obtained by applying the DR equation to the different adsorption measurements performed. The characteristic curves obtained for N₂, correspond to the experiments performed with an Omnisorp apparatus that cover relative pressures from 10⁻⁷ to 1. The affinity coefficient used in this case is 0.33 [9]. The characteristic curves for CO₂ adsorption contain the isotherms obtained up to sub-atmospheric and up to high pressures. The affinity coefficient for CO₂ has been calculated to have coincident characteristic curves for CO₂ and N₂ adsorptions, in those samples where the adsorption of this gas is not kinetically restricted. From this approach, the coefficient affinity calculated for CO₂ is 0.35, value similar to that proposed by Dubinin [9].

Figures 2 and 3 include two examples of characteristic curves obtained for samples CFC14 and CFC54 (plots of $\ln V$ vs $(A/\beta)^2$). These samples cover the different type of porosity found for the ACF studied. Sample CFC14 has a quite narrow porosity and N₂ adsorption has important diffusional problems. The porosity of sample CFC54 is well developed and contains some amount of supermicroporosity.

There are several relevant points that must be emphasized from Figures 2 and 3. In all the cases, the overlapping and continuation of the CO₂ characteristic curves obtained at low and high pressures is very good. For sample CFC14, the characteristic curve for N₂ adsorption remains always below that for CO₂, in agreement with the kinetically restricted adsorption for N₂ in this sample. With increasing the burn-off, the characteristic curve has not a unique slope and deviates upward. This reflects the development of porosity and the widening of the pore size distribution. This is clearly observed in Figure 3 that corresponds to sample CFC54. In this case, the characteristic curve for N₂ adsorption is very similar to the one for CO₂ obtained at high pressures (see the zone between 0-500 (kJ/mol)² in Figure 3). This indicates that CO₂ also fills the supermicroporosity that exists in this sample.

Finally, the characteristic curves for N₂ adsorption show in

all the samples a large deviation with respect to the one for CO₂ for values of $(A/\beta)^2$ higher than about 300 (kJ/mol)². In this zone, the volume of N₂ adsorbed by the sample is lower than the volume of CO₂ and decreases with increasing $(A/\beta)^2$. The adsorption potential, $(A/\beta)^2$, at which this deviation finishes depends on the burn-off of the sample. So, with increasing the burn-off, the recovery of the curve happens at higher $(A/\beta)^2$. This deviation, that happens at low relative pressures of N₂ (lower than 10⁻⁵ for sample CFC54 and lower than 10⁻⁴ for sample CFC14), shows that N₂ adsorption in the narrow microporosity is influenced by diffusional limitations. These experimental results are important by their relevance in the use of N₂ adsorption for the characterization of the porosity. As a consequence of the diffusional limitations, N₂ adsorption cannot be used to determine the micropore volume of the narrowest porosity, what makes necessary the use of other adsorptive to analyze this range of porosity. Hence, as already proposed [5], N₂ adsorption, complemented with CO₂ adsorption is an adequate procedure to determine the porosity of an activated carbon from the narrowest to the widest.

CONCLUSIONS

The results commented up to now show that CO₂ adsorption up to sub-atmospheric pressures can be used to calculate the volume of the narrow microporosity and that it is a convenient technique to complement the characterization of porosity through N₂ adsorption. CO₂ adsorbs in the super-microporosity when CO₂ pressures of about 4 MPa are used. The adsorption of N₂ at 77K is limited by diffusional problems that happen in the narrow porosity. For this reason, N₂ adsorption cannot be used to characterize this range of porosity that can be estimated by CO₂ adsorption.

Acknowledgements. The authors thank OCICARBON (project C-23-353) and DGICYT (project PB93-0945) for financial support and IBERDROLA for the Thesis Grant of J. Alcañiz-Monge.

REFERENCES

1. S.J. Gregg and K.S.W. Sing, *Adsorption, Surface Science and Porosity*. Academic Press (1982).
2. *Characterization of Porous Solids II*, (Eds. F. Rodriguez-Reinoso et al.) Elsevier Science Publishers B.V., Amsterdam (1991).
3. *Characterization of Porous Solids III*, (Eds. J. Rouquerol et al.) Elsevier Science Publishers B.V., Amsterdam (1994).
4. J. Rouquerol et al; *Characterization of Porous Solids III*, pp 1 (Eds. J. Rouquerol et al.) Elsevier Science Publishers B.V., Amsterdam (1994).
5. F. Rodriguez-Reinoso and A. Linares-Solano; *Chemistry and Physics of Carbon*, (Ed. P.A. Thrower) Vol. 21, 1. MARCEL DEKKER, NEW YORK (1988).
6. J. Garrido, A. Linares-Solano, J.M. Martín-Martínez, M. Molina-Sabio, F. Rodríguez-Reinoso and R. Torregrosa; *Langmuir*, 3, 76 (1987).
7. K. Kaneko, N. Setoyama and T. Suzuki; *Characterization of Porous Solids III*, pp.593 (Eds. J. Rouquerol et al.) Elsevier Science Publishers B.V., Amsterdam (1994).
8. J. Alcañiz-Monge, D. Cazorla-Amorós, A. Linares-Solano, S. Yoshida and A. Oya; *Carbon*, 32, 1277 (1994).
9. M.M. Dubinin; *Chemistry and Physics of Carbon*, (Ed. P.L. Walker) Vol. 2, 1. Marcel Dekker, New York (1966).

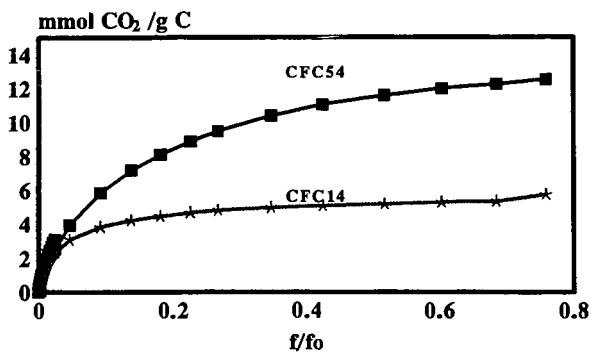


Figure 1. CO₂ adsorption isotherms.

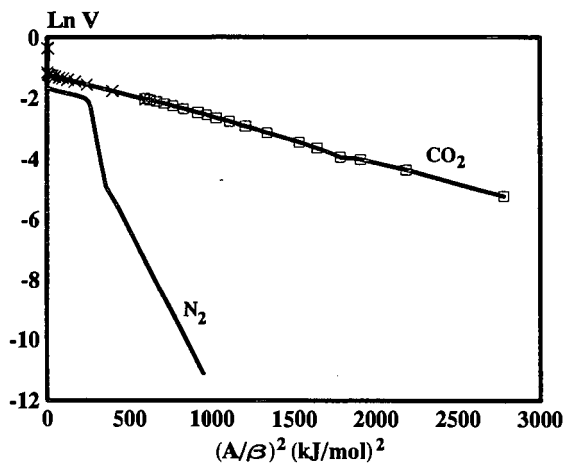


Figure 2. Characteristic curve of sample CFC14

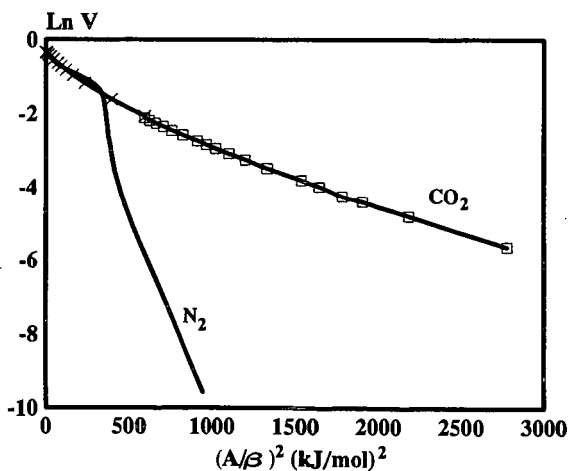


Figure 3. Characteristic curve of sample CFC54

OXIDATION OF SO₂ INTO RECOVERABLE Aq.H₂SO₄ OVER PITCH BASED ACTIVE CARBON FIBERS

Isao Mochida*, Keiichi Kuroda*, Yuji Kawabuchi*, Shizuo Kawano*, Akinori Yasutake†

Masaaki Yoshikawa††, and Yuji Matsumura††

*Institute of Advanced Material Study, Kyusyu University,

6-1 Kasugakoen, Kasuga-shi, Fukuoka 816, Japan.

†Nagasaki R and D Center, Mitsubishi Heavy Industry,

5-717-1 Fukabori, Nagasaki, 851-03, Japan.

††Research & Development Center, Osaka Gas Co., Ltd.,

6-19-9 Torishima, Konohana-ku, Osaka 554, Japan.

KEYWORDS : SO₂ removal, Active carbon fiber, Catalytic oxydation.

INTRODUCTION

The present authors have proposed a novel base for the removal of SO₂ in the flue gas where SO₂ is adsorbed, oxidized and hydrated over PAN-ACF to be continuously recovered in the form of aq. H₂SO₄. [1-3] Higher activity of ACF and less amount of humidity are wanted for smaller volume of the reactor, recovery of more concentrated H₂SO₄ and less consumption of water to reduce the cost of flue gas cleaning.

The present authors have found significant enhancement of the catalytic activity of PAN-ACF by the heat-treatment at 800°C. [4,5]

In the present study, catalytic activities of pitch based ACFs of high surface area were examined for the oxidative removal of SO₂. Pitch based ACF of as-received form has been reported to be inferior to PAN-ACF in the oxidative adsorption of SO₂. [5] However the heat-treatment is expected to enhance its catalytic activity. Hence the heat-treatment at rather high temperatures above 1000°C was examined to find higher activity. The hydrophobic surface of pitch based ACF can be expected to require smaller amount of H₂O for the complete removal of SO₂.

EXPERIMENTAL

OG series of pitch based ACF were supplied by Osaka gas Co.. It was heat-treated in nitrogen gas at several temperatures. Some of their properties are summarized in Table 1. SO₂ removal was carried out at 30°C, using a fixed bed flow reactor. Weights of ACF were 0.1 and 0.25g. The total flow rate was 100ml/min. The model flue gas containing SO₂ of 500-1000ppm, O₂ of 5vol% and H₂O of 5-20vol% in nitrogen was used. Aq.H₂SO₄ was recovered at the outlet of the reactor. SO₂ concentrations in the inlet and the outlet gases were observed continuously by a flame photometric detector (FPD) and NO_x gases were analyzed by NO_x meter (ECL-88US, Yanagimoto Co.,Ltd.).

Temperature programmed decomposition (TPDE) spectra of the ACFs were measured by using a quartz-glass apparatus equipped with a mass spectrometer (AQA-200, ANELVA INC.). The sample of 0.1g was heated in helium flow up to 1100°C with 10°C/min increments and the evolved gases such as CO and CO₂ were analyzed by the mass spectrometer.

RESULTS

The effects of heat-treatment temperature

Figure 1 illustrates the effects of heat-treatment temperature for SO₂ removal over pitch based ACFs. Stationary removal of SO₂ over all fibers was enhanced very much by the heat-treatment above 800°C. The activity was enhanced at higher temperature up to 1100°C. Complete removal was achieved for at least 15h with ACFs heat-treated above 900°C on OG-20A of the largest surface area. The ACF heat-treated at 1100°C removed completely SO₂ at W/F of 1x10⁻³ g min ml⁻¹. The Activity enhancement is remarkable. The large surface area provided the large activity after the heat-treatment among the ACF.

The activity of pitch based ACF OG-20A of the largest surface area

Figure 2 illustrates the desulfurization profiles of 1000ppm SO₂ by as-received and heat-treated OG-20A at W/F (Weight/Flow) = 1x10⁻³ g·min⁻¹·ml⁻¹, 10% humidity and 30°C. The favorable influences of the heat-treatment at higher temperature up to 1100°C were definite. The heat-treatment at 900°C and 1000°C increased the removal up to 40 and 80%, respectively. A further higher temperature of 1100°C removed completely SO₂ of 1000ppm for at least 15h. High temperature of 1200°C decreased the activity to 40% removal. There is certainly an optimum temperature of the heat-treatment with this particular OG-20A of very large surface area.

The effects of H₂O

Figure 3 illustrates the effects of H₂O in the SO₂ removal over OG-20A-HI100 by W/F of 1x10⁻³ g·min⁻¹·ml⁻¹ at 30°C. Lower concentration of H₂O decreased the extent of SO₂ removal, providing 100% removal at 10% H₂O, 96% at 7.5% H₂O, and 55% at 5% H₂O. Larger W/F of 5x10⁻³ g·min⁻¹·ml⁻¹ allowed complete removal with 5% H₂O.

The influence of NO

Figure 4 illustrates the influence of NO of 500ppm at SO₂ of 500ppm removal over pitch based ACFs by W/F of 2.5x10⁻³ g min ml⁻¹ at 30°C. Without NO, SO₂ was removed completely for longer than 20h. While a concentration of NO of 500ppm reduced the stationary removal of SO₂ to 35%. More H₂O and a larger W/F increased SO₂ removal in the presence of NO. NO leaked freely without any removal except for the initial 1h while its outlet concentration increased very sharply from 0 to 100%. No reaction of NO was estimated at the stationary state while NO

certainly inhibited the SO₂ removal by requiring larger H₂O concentration or W/F for the complete removal of SO₂.

TPDE spectrum of pitch based ACFs

Figure 5 shows the profiles of CO and CO₂ evolution from OG-20A, OG-15A, and OG-10A. CO₂ began to be evolved at about 180°C giving a highest evolution at 300°C, and then gradually decreased its amount to become null at 900°C regardless of the extent of activation of the fibers. CO began to be evolved at about 200°C and its amount increased gradually upto 500°C and then rapidly to 900°C where the maximum was observed. The amount of evolved CO increased with the increasing extent of activation and surface area. Significant retardation of NO without its stationary conversion should be studied in more details for scientific as well as technical view points.

DISCUSSION

The present study reported a remarkably high activity of a pitch based active carbon fiber of very large surface area after the heat-treatment at unusually high temperature of 1100°C. The activity observed in the present study allowed the complete removal of 1000ppm SO₂ at room temperature over OG-20A-H1100. A very small volume of reactor is designed by such a high activity. The active site for SO₂ removal is not identified. Large surface area and deoxygenated surface may provide more active sites of SO₂ oxidation and accelerate the elution of aq. H₂SO₄ with minimum H₂O from the active site because of high hydrophobicity.

REFERENCES

1. I. Mochida, S. Kisamori, S. Kawano, and H. Fujitsu, *Nippon Kagaku Kaishi*, **12**, 1429, (1992).
2. I. Mochida, T. Hirayama, S. Kisamori, S. Kawano, and H. Fujitsu, *Langmuir*, **8**, 2290, (1992).
3. S. Kisamori, I. Mochida, and H. Fujitsu, *Langmuir*, **10**, 1241, (1994).
4. S. Kisamori, S. Kawano and I. Mochida, *Chem. Lett.*, **11**, 1899, (1993).
5. S. Kisamori, K. Kuroda, S. Kawano, I. Mochida, Y. Matsumura and M. Yoshikawa, *ENERGY & FUELS*, **8**, 1337 (1994).

Table 1. Some Properties of Pitch Based Active Carbon Fibers.

ACFs	Ultimate analysis (wt%)					Surface area (m ² /g)
	C	H	N	O	Ash	
OG-5A	89.6	1.1	0.7	8.2	0.3	480
OG-15A	92.5	0.9	0.4	5.8	0.4	1550
OG-20A	93.9	0.9	0.3	4.6	0.5	1860
OG-20A-H900 ^{a)}	95.8	0.6	0.3	2.8	0.5	1690
OG-20A-H1100 ^{a)}	97.5	0.1	0.2	1.6	0.6	1570
OG-20A-H1200 ^{a)}	98.0	0	0.2	1.2	0.6	1420

a) Calcination temperature (°C)

OG-series: Pitch based active carbon fiber

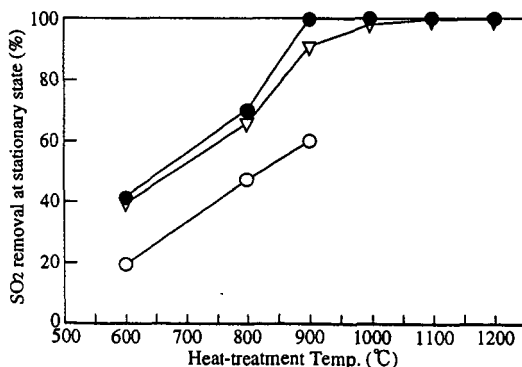


Figure 1 The effects of heat-treatment temperature for SO₂ removal over Pitch-ACFs

SO₂ 1000ppm, O₂ 5 vol%, H₂O 10 vol%

W/F = 2.5×10^{-3} g min mL⁻¹, Reaction Temp. 30°C

○: OG-5A (S.A. 480m²/g)

▽: OG-15A (S.A. 1550m²/g)

●: OG-20A (S.A. 1850m²/g)

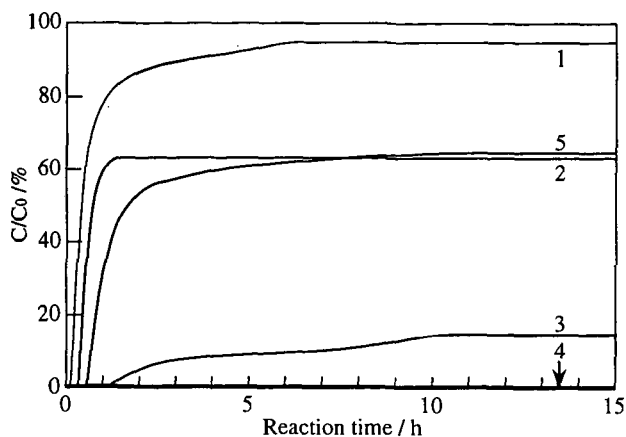


Figure 2 Breakthrough Profiles of SO_2 over Pitch-ACFs at 30°C
 SO_2 1000ppm, O_2 5 vol%, H_2O 10 vol%
 $\text{W/F} : 1.0 \times 10^{-3} \text{ g min mL}^{-1}$
 1: OG-20A
 2: OG-20A-H900
 3: OG-20A-H1000
 4: OG-20A-H1100
 5: OG-20A-H1200

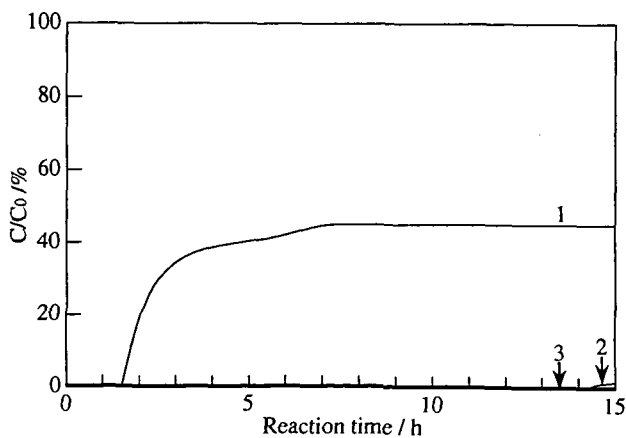


Figure 3. Breakthrough Profiles of SO_2 over Heat-treated Pitch-ACF at several H_2O concentration at 30°C
 SO_2 1000ppm, O_2 5 vol%, H_2O 10 vol%
 $\text{W/F} : 1.0 \times 10^{-3} \text{ g min mL}^{-1}$
 ACF: OG-20A-H1100
 H_2O 1: 5vol%, 2: 7.5vol%, 3: 10vol%

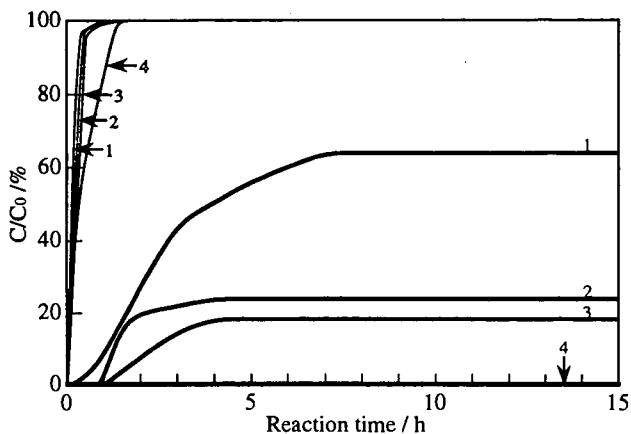


Figure 4 Breakthrough profiles of SO₂ and NO over OG-20-1100 at 30°C
 SO₂ : 500 ppm, NO : 500 ppm, O₂ : 5 vol%,
 W/F = $1.0 \times 10^{-3} \text{ g} \cdot \text{min} \cdot \text{ml}^{-1}$
 H₂O 1 : 10 vol%, 2 : 15 vol%, 3 : 20 vol%
 4 : W/F = $2.5 \times 10^{-3} \text{ g} \cdot \text{min} \cdot \text{ml}^{-1}$ H₂O : 10%

SO₂ : —
 NO : —

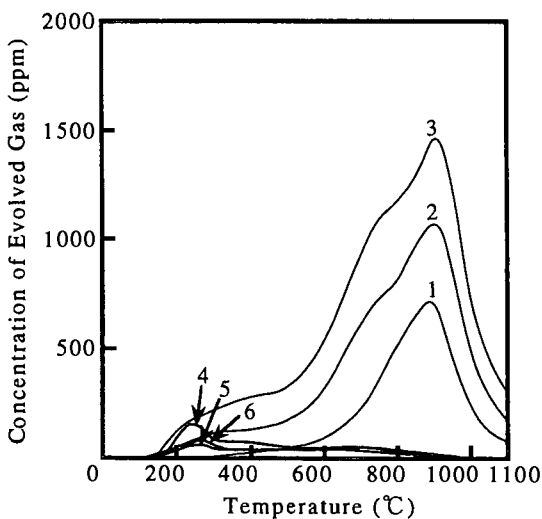


Figure 5 TPDE spectra of CO and CO₂ evolution from Pitch Based ACF
 Weight : 100mg
 Carrier gas : Helium
 Flow rate : 100ml/min

Sample	
CO	CO ₂
1 : OG-5A	4 : OG-5A
2 : OG-15A	5 : OG-15A
3 : OG-20A	6 : OG-20A

ADSORPTION OF SO₂ ON BITUMINOUS COAL CHAR AND ACTIVATED CARBON FIBER PREPARED FROM PHENOL FORMALDEHYDE

Joseph A. DeBarr^{1,2}, Anthony A. Lizzio¹ and Michael A. Daley³

¹Illinois State Geological Survey, 615 E. Peabody Dr., Champaign, IL 61820

²University of Illinois, Environmental Engineering and Science Program, Urbana, IL 61801

³University of Illinois, Materials Science and Engineering Department, Urbana, IL 61801

Keywords: Activated carbon fiber, coal char, SO₂ adsorption

INTRODUCTION

Carbon-based materials are used commercially to remove SO₂ from coal combustion flue gases. Historically, these materials have consisted of granular activated carbons prepared from lignite or bituminous coals [1-3]. Recent studies have reported that activated carbon fibers (ACFs) may have potential in this application due to their relatively high SO₂ adsorption capacity [4-6]. In this paper, a comparison of SO₂ adsorption for both coal-based carbons and ACFs is presented, as well as ideas on carbon properties that may influence SO₂ adsorption.

EXPERIMENTAL

Sample Preparation

The chars used in this work were prepared from an Illinois No. 2 hvCb coal, sample IBC-102 of the Illinois Basin Coal Sample Program [7]. A physically cleaned 48x100 mesh sample having 3.6% mineral content was prepared from the parent coal and used throughout as the feedstock for activated char. Chars were prepared at 900°C for 0.5 h in a 5 cm ID batch fluidized-bed reactor (FBR). In each run, 200 g IBC-102 coal was fluidized in flowing N₂ (6 L/min) and heated to the desired pyrolysis temperature. A multistep heating procedure was used to minimize agglomeration of coal particles in the FBR. Steam activation was done to develop microporosity and increase surface area further. Typically, 50 g of char was placed in the FBR and heated to 860°C in flowing N₂. The N₂ flow was replaced by 50% H₂O/50% N₂ (6 L/min) for 0.75 h to achieve 30% carbon conversion. In some cases, the H₂O-activated char was treated with nitric acid (HNO₃). Typically, 10 g of the char was added to 0.2 L 10 M HNO₃ solution, and refluxed at 80°C for 1 h. The HNO₃-treated carbon was washed with distilled H₂O to remove excess acid and vacuum dried overnight at 25°C. In some cases, the HNO₃-treated char was heated in N₂ to 525, 725, or 925°C and held for 1 h to remove oxygen placed on the carbon by the HNO₃ treatment.

ACFs with surface areas and oxygen contents ranging from 700 to 2800 m²/g and 0 to 5 wt%, respectively, were prepared commercially by reacting phenol formaldehyde fiber precursors (Kynol) in a steam/carbon dioxide mixture at temperatures between 700 and 900°C. ACFs with acidic and basic surface chemistry were prepared using methods described elsewhere [8,9].

Sample Characterization

The SO₂ adsorption capacities of samples were determined by thermogravimetric analysis (Cahn TG-131). In a typical run, a 30-50 mg sample was placed in a platinum pan and heated at 20°C/min in flowing N₂ to 360°C to remove moisture and impurities. The sample was cooled to 120°C. Once the temperature stabilized, the N₂ was replaced by a mixture of gases containing 5% O₂, 7% H₂O and the balance N₂. Once there was no further weight gain due to adsorption of O₂ and H₂O, SO₂ was added in concentrations representative of a typical flue gas from combustion of high sulfur coal (2500 ppmv SO₂). The weight gain was recorded versus time by a computerized data acquisition system.

Temperature programmed desorption (TPD) experiments were done in a flow-thru, 2.5 cm ID stainless steel fixed-bed reactor system. In a typical run, 0.5 g of sample was heated in flowing nitrogen (0.5 L/min) at 5°C/min to a final temperature of 1000°C and held for 1 h to achieve nearly complete desorption of CO and CO₂ from the carbon surface. Non-dispersive infrared analyzers (Rosemount Model 880) were used to monitor the concentrations of CO and CO₂ in the effluent gas continuously.

N₂ BET surface areas of chars were determined using a single point BET adsorption equation with N₂ (77 K) adsorption data obtained at a relative pressure (P/P₀) of 0.30 with a Monosorb flow apparatus (Quantachrome Corporation). Surface areas were determined for ACFs with a Micromeritics analyzer using nitrogen adsorption at 77K. Average pore sizes of ACFs were calculated using the Dubinin-Radushkevich equation and the nitrogen adsorption isotherm measured using a Coulter Omnisorb.

RESULTS AND DISCUSSION

Coal Chars

The results presented in Figure 1 suggest a lack of correlation between SO₂ adsorption and N₂ BET surface area. Two steam activated carbons prepared from IBC-102 with intermediate surface areas (200 and 360

m²/g) and a commercial activated carbon, Calgon F400 (1000 m²/g), adsorbed similar amounts of SO₂ (between 15 and 20 wt% SO₂) after about 4 hours. The Centaur carbon, which had the highest SO₂ adsorption capacity, had an N₂ BET surface area of only 360 m²/g. This carbon catalyst was developed by Calgon for both liquid and vapor phase applications, including removal of SO₂ and NO_x from flue gas. Figure 1 also shows that an activated carbon prepared from IBC-102 coal by steam activation, HNO₃-treatment and subsequent heat treatment to 925°C exhibited SO₂ adsorption behavior similar to the Centaur carbon. One study [10] showed that there was no correlation between the SO₂ adsorption capacity and surface area of a coal-based carbon, while another [11] has maintained that "surface area is the most important parameter in order to predict the behavior of a char in the abatement of SO₂ from exhaust gases."

A better understanding of SO₂ adsorption behavior may require more detailed information about the carbon-oxygen (C-O) complexes formed during char preparation and SO₂ adsorption. The authors showed previously a poor correlation between SO₂ adsorption capacity and the total amount of chemisorbed oxygen for chars prepared under a wide range of conditions [12-14]. Davini [15] also observed no correlation between SO₂ adsorption and chemisorbed oxygen. He found a better correlation between SO₂ capacity and the basic (or high temperature) C-O functional groups. In the current study, the steam activated char was found to have a surface populated predominantly by high temperature C-O complexes. To increase the number of high temperature C-O complexes, and presumably SO₂ capacity, the H₂O-activated char was treated with HNO₃ and thermally desorbed at temperatures ranging from 200 to 1075°C. Figure 2 presents the TPD profiles of the HNO₃-treated char and those thermally desorbed at 525, 725 and 925°C. The CO and CO₂ evolution profiles of the original HNO₃-treated char showed only slight overlap. Conceivably, this char could be heated in inert gas to a certain temperature, e.g., 525°C, to remove only the CO₂-forming functional groups and retain the CO-forming ones. Figure 3 shows that the SO₂ adsorbed increased with increasing thermal desorption treatment. A three-fold increase in SO₂ adsorption is observed with the relatively small increase in thermal desorption temperature from 525 to 725°C, and the char with the smallest amount of C-O complex (925°C) adsorbed the largest amount of SO₂. This suggests that sites that form a stable C-O complex during char preparation are made available by the thermal desorption treatment, and that adsorption of SO₂ may preferentially occur at these free adsorption sites. Using TPD, the authors previously measured the number of free adsorption sites for several carbons; a direct relationship was found between SO₂ capacity and free sites [12,14,16]. Based on these results, a reaction scheme was recently proposed to explain SO₂ removal by carbon whereby the free sites control the rate of adsorption of SO₂ and conversion to H₂SO₄ [17,18].

ACFs

Figure 4 shows that the SO₂ adsorbed varies inversely with surface area for the ACFs studied. The pore volumes of these ACFs are known to increase from about 0.3 (ACF-10) to 0.8 cm³/g (ACF-25) [19]. Others have also observed a decrease in adsorption of SO₂ with increasing surface area and micropore volume of ACF (polyacrylonitrile fibers) [4,6]. The oxygen and nitrogen (< 0.05%) content, although not measured directly for this series of ACF, should not have varied much among these four samples; although, the oxygen content of ACF-10 and 15 may have been slightly greater than that of ACF-20 and 25 [19,20]. Excluding the idea of free sites for now, the results presented in Figure 4 suggest that pore size was the most important factor for determining the SO₂ adsorption properties of these ACFs. These ACFs are known to have relatively narrow pore size distributions [20,21]. In this study, we calculated the average pore sizes of ACFs 10, 15, 20 and 25 to be 9.4 Å, 11.7 Å, 13 Å and 17.5 Å, respectively. Foster et al. [19] studied a series of ACF similar to those used in this study and found that for ppm levels of n-butane, benzene or acetone, low surface area ACF adsorbed more than high surface area ACF. It is well known that smaller pores are preferentially filled at low relative pressures (concentrations) of adsorbate due to the overlap of attractive forces of opposite pore walls. If a similar adsorption mechanism occurs in the SO₂-ACF system as in the n-butane-ACF system, this would explain the behavior observed in Figure 4, and help explain the lack of correlation between N₂ BET surface area and SO₂ capacity observed for the coal chars. Ultimately, the number of free sites as well as pore size distribution and pore volume of an activated carbon should define its SO₂ adsorption behavior. The relative importance of each remains to be determined.

Figure 5 shows that the ACF-10 treated with both sulfuric and nitric acids (H₂SO₄/HNO₃) and thermally desorbed to 400 and 700°C exhibits SO₂ adsorption behavior similar to that of the HNO₃-treated, thermally desorbed coal chars (Figure 3). The SO₂ adsorption capacity of the H₂SO₄/HNO₃ treated carbon thermally desorbed at 700°C is much greater than that of the original ACF-10. The presence of adsorbed O₂ on ACF may serve only to block access of SO₂ to free active sites, similar to the behavior we have observed for Illinois coal char. Heating the H₂SO₄/HNO₃-treated ACF to 700°C would gasify part of the ACF, evolving oxygen as CO or CO₂, thus increasing the average pore size. If the average pore size of ACF increases with oxidation/thermal desorption, the results shown in Figure 4 would predict a decrease in the SO₂ capacity of H₂SO₄/HNO₃ treated ACF thermally desorbed at 700°C, if pore size was the only controlling factor. The fact that there was an increase in SO₂ adsorption despite an increase in pore size suggests the strong influence of free sites in controlling SO₂ adsorption behavior. It remains to be determined whether the free site concentration of these ACFs can be measured. It is interesting that the thermal desorption treatment applied to both the H₂SO₄/HNO₃-treated ACF and the HNO₃-treated coal char serves to increase not only the SO₂ adsorbed, but also the initial rate of SO₂ adsorption (Figures 3 and 5); this behavior has been attributed to an increase in the number of active sites [22].

Modifying the surface chemistry of ACFs by incorporating different functional groups has been shown to improve adsorption of various adsorbates [8,9,19,20,23,24]. ACFs with both acidic and basic surfaces, and an average pore size smaller than the original ACF-10, were prepared using methods described in previous work [8,9]. Since SO_2 is an acid gas, a carbon with basic surface characteristics would be expected to exhibit enhanced SO_2 adsorption. Indeed, Figure 6 shows that a basic ACF adsorbs more SO_2 than an acidic ACF. Others have also suggested that the presence of small amounts of nitrogen in ACF can markedly improve its SO_2 removal capabilities [4,6,25,26]. Work is in progress to learn how the interrelationships among number of free sites, pore size distribution and types of functional groups may control a carbon's SO_2 adsorption behavior [27].

CONCLUSIONS

Coal-based activated carbons and ACFs, prepared by a novel oxidation/thermal desorption treatment, had SO_2 adsorption capacities approaching that of a commercial carbon catalyst. The current price of ACFs, about \$10/lb., may limit their use in SO_2 removal applications, however, some recent work suggests that ACFs can be prepared for \$1- \$2/lb. [28]. Further work is needed to characterize these less expensive ACF systems for SO_2 removal. The results obtained in this study suggest that pore size as well as the number of free active sites play important roles in determining a carbon's SO_2 adsorption capacity. The complete pore size distributions of the treated coal-based carbons and ACFs remain to be determined; these should provide additional insight into the relative importance of pore size and free sites in controlling SO_2 adsorption behavior. The use of functional groups, e.g., nitrogen-containing ones, to modify a carbon's surface to improve SO_2 adsorption appears promising, and is also an area for further investigation.

ACKNOWLEDGMENTS

This work was sponsored by the Illinois Department of Energy and Natural Resources through the Illinois Coal Development Board and Illinois Clean Coal Institute, and the United States Department of Energy. The technical assistance of Ms. Gwen Donnals is gratefully acknowledged. Discussions with Dr. Mark Rood, Dr. Carl Kruse and Dr. John Lytle are appreciated.

REFERENCES

1. Richter, E., Knoblauch, K., Jungten, H., 1987, *Gas Sep. Purif.* 1, p. 35.
2. Tsuji, K., Shiraiishi, I., 1991, "Mitsui-BF Dry Desulfurization and Denitrification Process using Activated Coke," Proceedings of the EPRI SO_2 Control Symposium, Washington, D.C., p. 307.
3. Brueggendick, H., Pohl, F.G., 1993, "Operating Experience with STEAGs Activated Carbon Processes - a/c/tTM - In European Waste Incinerator Plants," Proceedings of Tenth Annual International Pittsburgh Coal Conference, p. 787.
4. Mochida, I., Hirayama, T., Kismori, S., Kawano, S., Fujitsu, H., 1992, *Langmuir* 8, p. 2290.
5. Kismori, S., Mochida, I., Fujitsu, H., 1994, *Langmuir* 10, p. 1241.
6. Kim, J.Y., Hong, I., Lee, J.G., 1995, "Influences of Preparation Conditions of ACF on Catalytic Activity for SO_2 Removal," Proceedings of 22nd Biennial Conference on Carbon, San Diego, CA, p. 534.
7. Harvey, R.D., Kruse, C.W., 1988, *J. Coal Qual.* 7, p. 109.
8. Economy, J., Foster, K., Andreopoulos, A. and Jung, H., 1992, "Tailoring Carbon Fibers for Adsorbing Volatiles," *Chem Tech*, p. 597.
9. Economy, J., Daley, M.A. and Mangun, C.L., 1996, "Activated Carbon Fibers - Past, Present and Future," ACS Preprints, Fuel Chem. Div., New Orleans, LA.
10. Davini, P., 1989, *Fuel* 68, p. 145.
11. Rubio, B., Izquierdo, M.T., Mastral, A.M. and Mayoral, C., 1994, "Proceedings of International Conference on Carbon, "Use of Low Rank Coal Chars in the Abatement of SO_2 from Flue Gases," Granada, Spain, p. 402.
12. Lizzio, A.A., DeBarr, J.A., Donnals, G.L., Kruse, C.W., Rood, M.J., Gangwal, S.K., 1995, "Production and Use of Activated Char for Combined SO_2/NO_x Removal," Final Technical Report, Illinois Clean Coal Institute, Carterville, IL.
13. DeBarr, J.A. and Lizzio, A.A., "Production of Activated Char for Combined SO_2/NO_x Removal," Proceedings of International Conference on Carbon, Granada, Spain, 1994, p. 268.
14. Lizzio, A.A. and DeBarr, J.A., "Effect of Surface Area and Chemisorbed Oxygen on SO_2 Adsorption Capacity of Activated Char," *Fuel* 1996 (in press).
15. Davini, P., 1990, *Carbon* 28, p. 565.
16. DeBarr, J.A., 1995, "The Role of Free Sites in the Removal of SO_2 from Simulated Flue Gases by Activated Char," M.S. Thesis, University of Illinois, Urbana, IL.
17. DeBarr, J.A. and Lizzio, A.A., 1995, "New Insights on the Mechanism of SO_2 Removal by Carbon," Proceedings of 22nd Biennial Conference on Carbon, San Diego, CA, 1995, p. 562.
18. Lizzio, A.A., DeBarr, J.A., 1996, "The Mechanism of SO_2 Removal by Carbon," ACS Preprints, Fuel Chem. Div., New Orleans, LA.
19. Foster, K.L., Fierman, R.G., Economy, J., Larson, S.M., Rood, M.J., 1992, *Chem. Mater.* 4, p. 1068.
20. Cal, M.P., 1995, "Characterization of Gas Phase Adsorption Capacity of Untreated and Chemically Treated Activated Carbon Cloths," Ph.D. Thesis, University of Illinois, Urbana, IL.
21. Lin, R.Y., Economy, J., 1973, *Applied Polymer Symposium* 21, p. 143.
22. Jungten, H. and Kuhl, H., 1989, *Chem. Phys. Carbon* 22, p. 145.

23. Cal, M.P., Dimotakis, E.D., Economy, J., Larson, S.M. and Rood, M.J., 1996, "The Effect of Chemical Modification of Activated Carbon Cloth on the Adsorption Capacity of Organics and Water Vapor," ACS Preprints, Fuel Chem. Div., New Orleans, LA.
24. Daley, M.A., Mangun, C.L., Economy, J., 1996, "Predicting Adsorption Properties for ACFs," ACS Preprints, Fuel Chem. Div., New Orleans, LA.
25. Nishijima, A., Kurita, M., Kiyozumi, Y., Kobayashi, R., Hagiwara, H., Ueno, A., Sato, T., Todo, N., 1980, *The Chemical Society of Japan* 53, p. 3356.
26. Fei, Y., Sun, Y.N., Givens, E., Derbyshire, F., 1995, "Continuous Removal of Sulfur Oxides at Ambient Temperature, using Activated Carbon Fibers and Particulates," ACS Preprints, Fuel Chem. Div., 40 (4), p. 1051.
27. DeBarr, J.A., 1996, Ph.D. Thesis, University of Illinois, Urbana, IL.
28. Daley, M., 1996, Ph.D. Thesis, University of Illinois, Urbana, IL.

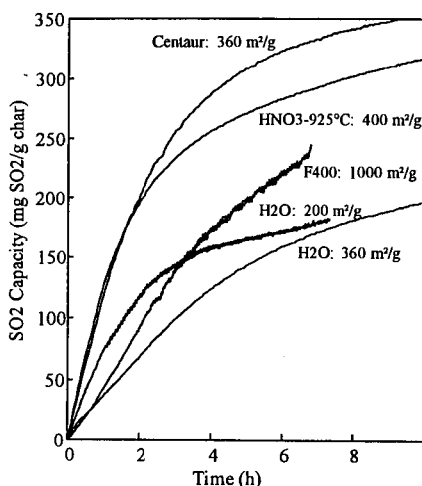


Figure 1. Effect of N₂ BET surface area on SO₂ adsorption capacity of selected IBC-102 chars and commercial carbons.

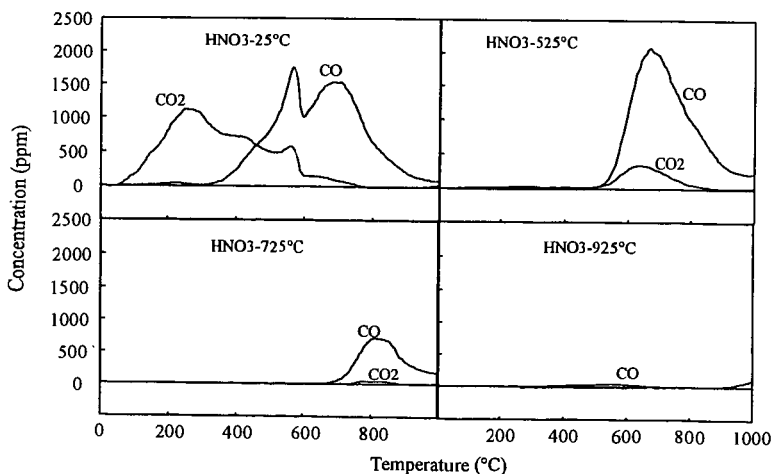


Figure 2. TPD profiles of nitric acid treated/thermally desorbed IBC-102 chars.

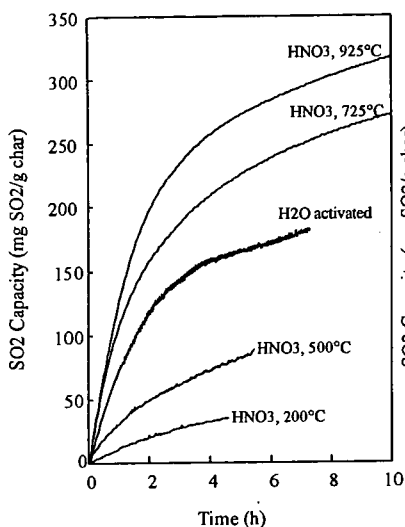


Figure 3. SO₂ adsorption for HNO₃-treated chars desorbed to different temperatures.

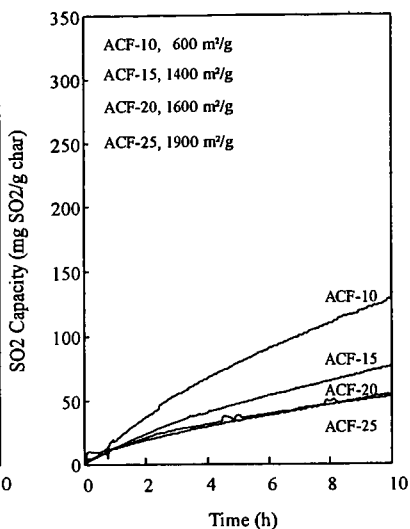


Figure 4. SO₂ adsorption for ACFs.

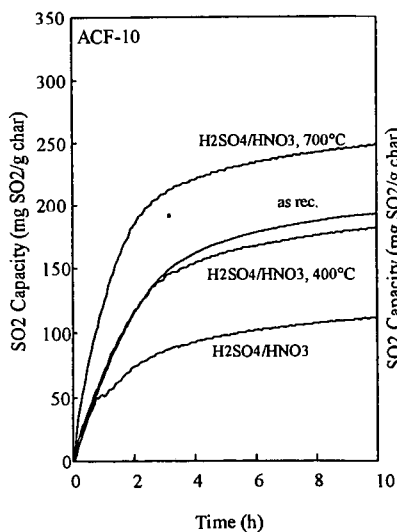


Figure 5. SO₂ adsorption for oxidized ACFs desorbed to different temperatures.

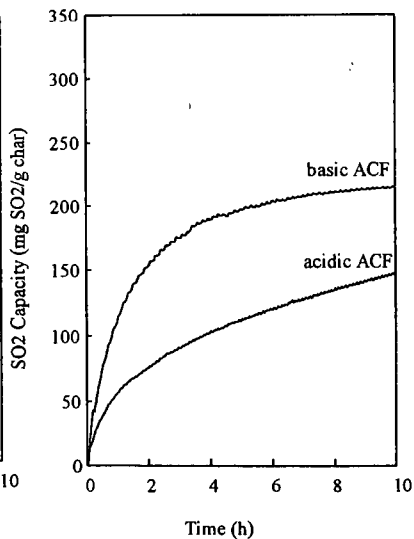


Figure 6. SO₂ adsorption for acidic and basic ACF.

THE EFFECT OF CHEMICAL MODIFICATION OF ACTIVATED CARBON CLOTH ON THE ADSORPTION CAPACITY OF ORGANICS AND WATER VAPOR

Mark P. Cal¹, Emmanuel D. Dimotakis², James Economy², Susan M. Larson³, and Mark J. Rood³

University of Illinois at Urbana-Champaign, Urbana, IL 61801

¹P.O. Box 70400, Reno, NV, e-mail: markc@sage.dri.edu

²Department of Materials Science and Engineering

³Environmental Engineering and Science Program, Department of Civil Engineering

Keywords: adsorption, activated carbon, chemical treatment.

INTRODUCTION

In an effort to maximize VOC adsorption, particularly in the case of compounds which are not readily adsorbed on activated carbon cloth (ACC), e.g., acetaldehyde, and to minimize the adsorption of water vapor, several chemical treatments were performed on virgin ACC-20. A sulfuric/nitric acid treatment produced a highly oxidized surface; chemical treatment with NH₃ produced a basic surface and increased the nitrogen content of the ACC; and finally, Cl₂ was used to produce a polar surface. Adsorption isotherms were measured for acetaldehyde, benzene, and water vapor to observe the effect on adsorption capacity for chemically treated ACC-20.

EXPERIMENTAL PROCEDURES

The starting material, ACC-20, was obtained from Nippon Kynol, Inc. Characteristics of the untreated and chemically modified ACC-20 samples are presented in Table 1. A brief summary of the experimental procedures used in this research is presented below. For a more detailed description of experimental procedures, please consult Dimotakis et al., 1995 and Cal, 1995.

Modification of ACC-20 with Ammonia or Chlorine

About 1.0 g of ACC-20 was placed in a 5-cm i.d. temperature-controlled quartz tubular furnace. The tube was purged with N₂ for 5 min, the temperature was increased to 180°C for 15 min, and then at the desired reaction temperature NH₃ or Cl₂ were introduced for the necessary reaction period. After completion, the gas was replaced with nitrogen, and the sample was cooled to room temperature. The samples were stored in closed vials prior to analysis.

Oxidation of ACC-20

The oxidation reactions were performed by immersing 1.45 g of ACC-20 in 100 ml of 1/1 (v/v) HNO₃/H₂SO₄ solution for two time periods: 10 min and 4 days. Gas evolution was observed during treatment. After the treatment, the product was washed with distilled water and left to dry overnight. Twelve hours later, it was dried at 150°C with N₂ for 30 min and then was stored in closed vials.

X-Ray Photoelectron Spectroscopy (XPS) Measurements

XPS was used to determine the elemental content (O, N, Cl and C) of the surface of the treated and untreated ACC samples (Briggs and Seah, 1983). The work was carried out at the Materials Research Laboratory of the University of Illinois at Urbana-Champaign, using a PHI 5400 (Perkin-Elmer, Physical Electronics Inc.) instrument. Mg-K α radiation and a power of 400 Watts at 15 kV were used. The samples were dried at 150°C for 30-45 min prior to analysis since the technique requires ultrahigh vacuum (10⁻⁸ to 10⁻¹⁰ torr). To analyze for the surface groups the carbon region of the XPS spectrum was deconvoluted to individual peaks (Table 2). XPS techniques were used to characterize the chemical changes on the surface of the fiber down to about 30 Å to 100 Å which is the maximum depth that the emitted photoelectrons can escape and be detected (Briggs and Seah, 1983). XPS can identify the N, Cl or O groups present based on their binding energy values. It was assumed that the chemical nature of the surface is similar to that of the core of the sample. Table 2 describes the percent of total carbon area of each group as a function of the binding energy (variations within 0.7 eV are observed for the treated samples): phenol or ether (285 eV), carbonyl (287 eV), carboxylic (288.8 eV) and unsaturated bond transitions (291.1 eV, also known as shake-up peaks) (Foster, 1993).

Organic and Water Vapor Adsorption Isotherms

Acetaldehyde, benzene, and water vapor adsorption isotherms for the ACC samples were measured gravimetrically using a Cahn microbalance (Model C-2000). The gas stream for the organic compound of interest was generated using a certified gas cylinder of known organic concentration, diluted with hydrocarbon-free air using mass flow controllers (Tylan Model FC-280) to obtain the desired concentrations. To generate gas streams with different relative humidities, a membrane humidifier was used in combination with a dew-point hygrometer (Cal, 1995). The adsorption isotherms were measured at 25°C and a total pressure of about 1 atm. ACC sample masses were between 10 and 20 mg and the total gas flow rate through the gravimetric balance was 0.1 to 0.25 L/min.

Acetaldehyde Adsorption

Acetaldehyde typically has a low adsorption capacity on activated carbons, including ACC. Therefore, any chemical treatment that could substantially enhance the adsorption of acetaldehyde (and similar compounds, such as formaldehyde) could be potentially useful. Comparison of the adsorption capacities (at 25°C and 1 atm total pressure) for a series of chemically modified ACC-20 samples that were untreated, oxidized, nitrated and chlorinated as described by Table 2 are presented in Figure 1.

The largest gas-phase acetaldehyde concentration in air examined was 500 ppmv, while 1000 ppmv was the highest concentration of acetone and benzene studied. It was observed that acetaldehyde undergoes conversion to acetic acid at higher concentrations, making the adsorption capacity measurements invalid (Venugopal et al., 1967; Matheson Gas, 1993). The highly oxidized sample, ACC20-(32% O), exhibits a much higher adsorption capacity for

acetaldehyde in the 50 to 500 ppmv concentration range when compared to untreated ACC-20. At 50 ppmv ACC20-(32% O) adsorbs 400% more acetaldehyde than untreated ACC-20 and at 500 ppmv it adsorbs 130% more acetaldehyde. The less oxidized sample, ACC20-(21% O), also shows enhanced acetaldehyde adsorption similar to that of ACC20-(32% O).

The increase in acetaldehyde adsorption capacity on oxidized ACC is theorized to be due to an increase in dipole interactions and hydrogen bonding that occurs between the acetaldehyde molecules and the additional carboxylic groups present on the oxidized ACC-20 (Table 1). This effect appears to be most pronounced at lower adsorbate concentrations, and diminishes at higher adsorbate concentrations, when the larger adsorbent pores begin to fill. It has been reported in the literature that surface oxygen groups can affect adsorption (Zawadzki, 1981; Boehm, 1966; Szymanski and Rychlicki, 1991).

Nitrated ACC20-(4% N) shows improved acetaldehyde adsorption capacity over untreated ACC-20 of 51% at 50 ppmv and 9% at 500 ppmv. This increase in adsorption capacity may be due to interaction with the basic surface or may be due to the change in pore structure of the ACC. Finally, in the case of the chlorinated ACC20-(7.8% Cl) a slight decrease in the adsorption capacity is observed compared to the untreated ACC. The decrease in adsorption capacity appears to be related to the ACC surface chemistry instead of physical properties because the pore volume is similar to that of ACC20-(21% O) (Table 1).

Benzene Adsorption

Adsorption isotherms for benzene and the series of chemically modified ACC are presented in Figure 2. Since benzene is nonpolar and essentially immiscible in H₂O, a hydrophilic surface should result in decreased adsorption (Puri et al., 1973). Oxidation of the ACC resulted in a 34% decrease in adsorption capacity for 1000 ppmv benzene in air, which is the same as the observed decrease in surface area (Figure 2 and Table 1). Therefore, oxidation had little or no effect on benzene adsorption, but rather the difference in adsorption capacity is due to changes in surface area and/or pore volume between ACC20-(3.9% O) and ACC20-(32% O). The nitrated (basic) surface shows a slight increase in benzene adsorption capacity, while the chlorinated ACC20-(7.8% Cl) showed a slight decrease in adsorption capacity as compared to ACC20-(3.9% O). This decrease in adsorption capacity may be attributable to the decrease in micropore volume observed on the chlorinated ACC samples or may also be attributed to experimental error in the measurements (Table 1).

Water Vapor Adsorption on Chemically Modified ACC

The adsorption of water vapor on ACC20-(32% O) differs significantly from the usually observed type V isotherm, and more closely resembles a type II isotherm (Figure 3). ACC20-(32% O) is expected to have many more oxygenated or hydrophilic sites than any of the other ACC due to its high oxygen content. The XPS data in Table 2 shows a higher number of carboxylic bonds than the untreated ACC-20, confirming that some of the hydroxyl and carbonyl bonds were oxidized to carboxylic bonds. The XPS data also shows that more carbon-oxygen (hydrophilic) bonds were formed during oxidation compared to untreated ACC-20. The increase in carboxylic groups may be responsible for the enhanced water vapor adsorption at low relative humidities (RHs). From Table 2 and the adsorption isotherm data, it appears that carboxylic groups have the most influence on water vapor adsorption at low RH. The difference between the adsorption and desorption curves (hysteresis) is not as pronounced here, as it is for the untreated ACC. This may be due to the increase in hydrogen-bonding between water and the oxidized carbon, allowing removal of water molecules in a more continuous manner.

Adsorption-desorption isotherms for nitrated ACC20-(4.1% N) are presented in Figure 3. ACC20-(4.1% N) exhibits an increase in water vapor adsorption capacity (200 to 600%, depending upon the RH) in the lower RH range (RH < 50%). This may be due to the increase in carboxylic sites compared to untreated ACC20-(3.9% O), as represented in the XPS data in Table 2. It has also been suggested that nitrogen can also constitute polar sites for H₂O_g adsorption (Bradley and Rand, 1993; Tomlinson, et al., 1993), thereby increasing H₂O_g adsorption at low RH. ACC20-(4.1% N) exhibits about a 10% higher water vapor adsorption capacity than ACC20-(3.9% O) at high RHs. This is due to the increased total pore volume of ACC20-(4.1% N) observed in Table 1. The widening in the adsorption hysteresis curve in for ACC20-(4.1% N) in Figure 3 is most likely due to a change in pore size distribution.

Adsorption isotherms for water vapor and chlorinated ACC are presented in Figure 4. Table 1 shows a decrease in BET surface area, a decrease in carbon content (in wt%), and a slight increase in oxygen content with increasing chlorination. The decrease in surface area may be due to chlorine atoms limiting or closing off access to the smaller micropores present on the ACC. Water vapor adsorption was decreased at RHs < 60% and where capillary condensation occurred (the step rise in the adsorption curve) was shifted to higher RHs for the chlorinated ACCs. The amount of water vapor adsorbed at saturation was decreased to a due to a decrease in pore volume (Table 1). While chlorination increases the amount of polar sites present on the ACC due to the addition of chlorine atoms, these sites do not appear to be favorable for water adsorption, as are carboxylic sites. Chlorination appears to increase the hydrophobicity of ACC.

SUMMARY

ACC-20 was chemically modified, producing oxidized, chlorinated, and nitrated samples. Adsorption capacities for VOCs in the 10 to 1000 ppmv concentration and water vapor from 0 to 95% RH were measured. Oxidized ACC-20 showed an enhanced physical adsorption for acetaldehyde and water vapor, probably due to increased dipole-dipole interactions and hydrogen bonding. Oxidation of ACC-20 changed the shape of the water vapor adsorption isotherm, so that it no longer resembles a Brunauer type V. Benzene showed a decreased adsorption capacity (about 20 to 30% less, depending upon concentration) on oxidized ACC-20, which may be due to and increase in hydrophobicity of ACC-20, or a change in pore size distribution. Nitridation of ACC showed little effect on organic adsorption capacity, but increased the saturation adsorption capacity for water vapor by 10% on ACC-20 and increased the breadth of its hysteresis loop. These changes were the result of changes in the pore size distribution of ACC-20.

ACKNOWLEDGEMENTS

This research was supported through grants from the Center for Indoor Air Research (Grant 91-03), the Hazardous Waste Research and Information Center (Grant ENR HWR 94-115), and the Advanced Environmental

Control Technology Research Center (Grant EPA CR 812582). We would also like to thank Richard T. Haasch of the Materials Research Laboratory of the University of Illinois at Urbana-Champaign for his assistance in analyzing the XPS data.

REFERENCES

- Boehm, H.P., *Adv. Catal.*, **16**:179, 1966.
- Bradley, R.H., and Rand, B., "The Adsorption of Vapours by Activated and Heat-Treated Microporous Carbons. Part 2. Assessment of Surface Polarity Using Water Adsorption," *Carbon*, **31**(2): 269-272, 1993.
- Briggs, D., and Seah, M.P., *Practical Surface Area Analysis by Auger and X-ray Photoelectron Spectroscopy*, John Wiley and Sons, New York, 1983.
- Cal, M.P., "Characterization of Gas Phase Adsorption Capacity of Untreated and Chemically Treated Activated Carbon Cloths," Doctoral Dissertation, University of Illinois at Urbana-Champaign, Environmental Engineering and Science Program, UMI Press, 1995.
- Dimotakis, E.D., Cal, M.P., Economy, J., Rood, M.J., Larson, S.M., "Chemically Treated Activated Carbon Cloths (ACCs) for Removal of VOCs from Gas Streams: Evidence for Enhanced Physical Adsorption," *Environmental Science and Technology*, **29**(7): 1876-1880, 1995.
- Dimotakis, E.D., Cal, M.P., Economy, J., Rood, M.J., Larson, S.M., "Water Vapor Adsorption on Chemically Treated Activated Carbon Cloths," accepted for publication to *Chemistry of Materials*.
- Foster, K.L., "The Role of Micropore Size and Chemical Nature of the Pore Surface on the Adsorption Properties of Activated Carbon Fibers," Doctoral Dissertation, University of Illinois at Urbana-Champaign, Department of Material Science and Engineering, 1993.
- Gregg, J. and Sing, K.S.W., *Adsorption, Surface Area and Porosity*, 2nd ed., Academic Press, London, 1982.
- Matheson Gas, personal communication, 1993.
- Puri, B.R., Kaistha, B.C., Vardan, Y., and Mahajan, O.P., *Carbon*, **11**: 329-336, 1973.
- Syzmanski, G. and Rychlicki, G., "Importance of Oxygen Surface Groups in Catalytic Dehydration and Dehydrogenation of Butan-2-ol Promoted by Carbon Catalysts," *Carbon*, **29**(4/5): 489-498, 1991.
- Tomlinson, J.B., Freeman, J.J., and Theocharis, C.R., "The Preparation and Adsorptive Properties of Ammonia-Activated Viscose Rayon Chars," *Carbon*, **31**(1): 13-20, 1993.
- Venugopal, B., Kumar, R., and Kuloor, N.R., "Oxidation of Acetaldehyde to Acetic Acid in a Sparger Reactor," *I&EC Process Design and Development*, **6**(1): 139-146, 1967.
- Zawadzki, J., "IR Spectroscopy Investigations of Acidic Character of Carbonaceous Films Oxidized with HNO_3 Solution," *Carbon*, **19**:19-25, 1981.

Table 1. Physical Characteristics and Elemental Composition of ACCs.

ACC-20 Chemical Treatment	BET Surface Area [m ² /g]	Total Pore Volume [cm ³ /g]	Micropore Volume [cm ³ /g]	C [wt%]	H [wt%]	N [wt%]	O [wt%]	Cl [wt%]
3.9% O/untreated	1550	0.74	0.61	95.40 95.97 ^a	0.68	0.05	3.92 4.03 ^a	0
4.1% N (nitridated)	1738	0.84	0.59	91.96 94.34 ^a	0.27	4.50 4.06 ^a	3.23 1.60 ^a	0
7.8% Cl (chlorinated)	1523	0.73	0.54	87.71	0.06	0.27	4.15	7.8
16% Cl (chlorinated)	1374	0.66	0.51	77.93 88.94 ^a	0.01	0.06	6.00 3.27 ^a	16 7.8 ^a
21% O (oxidized)	1409	0.66	0.55	76.26 85.53 ^a	1.41	1.49	20.84 13.84 ^a	0
32% O (oxidized)	1105	0.47	0.35	64.76 76.60 ^a	1.55	0.72	32.32 23.39 ^a	0

a. % Elemental as determined by XPS. Difference in Cl values between the two methods may be due to uncertainty in the calibration standard used.

Table 2. XPS Deconvolution of the Carbon 1s Peak Area for Chemically Modified ACC-20.

Binding Energy [eV]	Percentage of Total Area of Carbon Peak					
	3.9% O (untreated)	21% O	32% O	12.3% Cl	16% Cl	4.1% N
285 (C-C, C-H)	50.94	55.9	46.86	57.28	42.08	48.43
286 (phenol, hydroxyl, C-OH)	27.87	14.92	24.68	21.00	31.12	24.20
287 (carbonyl, C=O)	9.29	13.03	7.64	8.12	8.23	8.14
289 (carboxylic, C=OOH)	5.58	9.99	14.59	7.16	8.56	7.90
291 (shake-up band, $\Pi \rightarrow \Pi^*$)	6.32	6.15	6.23	6.43	10.00	11.35

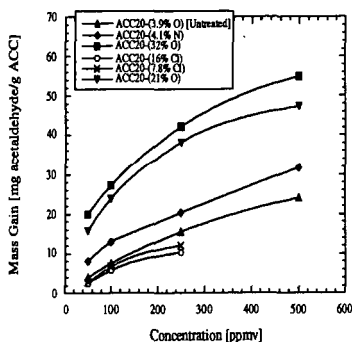


Figure 1. Adsorption of Acetaldehyde on Chemically Modified ACC.

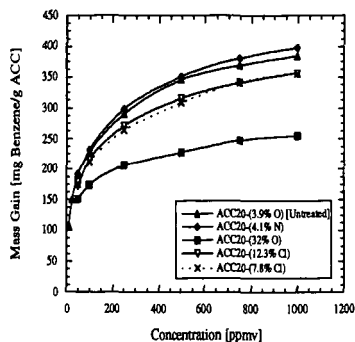


Figure 2. Adsorption of Benzene on Chemically Modified ACC.

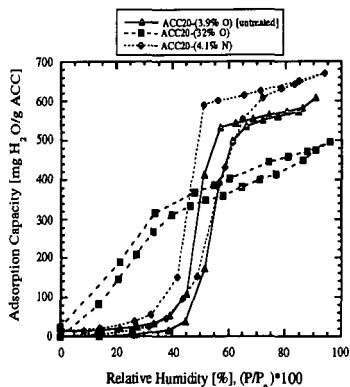


Figure 3. Adsorption and Desorption of Water Vapor on Oxidized and Nitrated ACC-20.

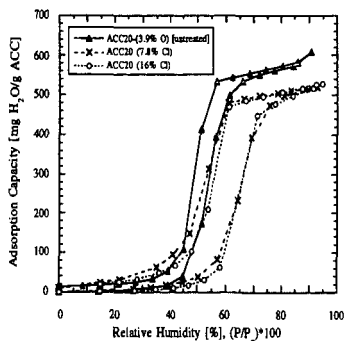


Figure 4. Adsorption and Desorption of Water Vapor on Chlorinated ACC-20.

PRODUCTION OF VAPOR GROWN CARBON FIBER
WITH COAL FINES WITHOUT SO₂ EMISSIONS

D. Burton, M. Lake, and R. Ali
Applied Sciences, Inc.
P.O. Box 579
Cedarville, OH 45314

Keywords: SO₂ Control Technologies, Coal Pyrolysis, Vapor Grown Carbon Fibers

ABSTRACT

Each year millions of tons of low-cost hydrocarbons in the form of coal fines are impounded. One potential application would be utilization in a unique process capable of converting the carbon into a highly graphitic vapor-grown carbon fiber (VGCF). This process currently produces vapor-grown carbon fiber from the vapor phase using natural gas, hydrogen sulfide and iron particles. The iron particles initiate the growth of the carbon fibers while the hydrogen sulfide enhances the yield, allowing the process to be economically feasible. Previous demonstrations involving pulverized coal have proven that coal can be used as an alternative source of carbon and sulfur in the production of VGCF. Furthermore, there is evidence that the sulfur from the coal remains with the carbon fiber catalyst during the reaction and does not exhaust as SO₂ into the atmosphere. It is the object of this research to determine if coal fines pulverized to -325 mesh are also a viable source of carbon and sulfur for VGCF production.

INTRODUCTION

Currently, commercial carbon fibers possessing a wide range of properties are formed from precursors of polyacrylonitrile (PAN) or petroleum pitch. Generally, these types of fibers have common methods of synthesis and handling, the latter of which is similar to textiles. Commercial fibers are made by extruding or spinning a continuous filament or thread from a polymer. The continuous filament is subsequently oxidized under tension to 200°C then carbonized by slowly heating it in the absence of air to 1000°C. Additional heating up to 3000°C provides higher degrees of graphitization necessary for ultra-high strength and/or stiffness applications. The cost of multi-step production for commercial carbon fibers limits their application to reinforcements in aerospace composites, golf clubs, fishing poles and other high performance products.

The production method of vapor grown carbon fibers is in sharp contrast to the production method of commercial carbon fiber. The one-step process, shown in Figure 1, has no involved extrusion or spinning operations allowing VGCF to be produced at a significantly lower cost. One type of vapor grown carbon fiber produced in our laboratory, and designated as PYROGRAF III, is initiated with iron particles which catalyze the growth of partially graphitic filaments in the presence of hydrocarbons at 1000-1100°C. Such fibers have diameters on the order of nanometers. Pyrocarbon subsequently deposited on the walls of the filament thickens the diameter of the fiber with the basal planes of the deposited carbon preferentially oriented parallel to the filament surface¹. Recent studies have shown significant enhancement of fiber nucleation efficiency by the addition of sulfur into the reaction². The sulfur reacts with the catalyst and becomes overcoated by the fiber. Although H₂S is beneficial to the efficiency of fiber production, it is used with great reluctance since it is expensive, highly corrosive to rubber seals and metal fittings, flammable, and as toxic as hydrogen cyanide. Therefore, coal fines are being trialed as the source of sulfur to eliminate the hazards and high cost of hydrogen sulfide.

Figures 2 and 3 show scanning electron micrographs of PYROGRAF III and typical continuous commercial carbon fibers. The diameter of PYROGRAF III generally averages 0.2µm as produced while commercial fibers are 8µm in diameter. Unlike commercial fibers, PYROGRAF III are not continuous but are an entangled mass resulting from the

turbulence of their gas phase generation. The length/diameter ratio for PYROGRAF III ranges from 40 to 200. However, due to the purity with which carbon is incorporated into the fiber, VGCF has a highly graphitic structure which results in higher values of physical properties than are realized in commercial carbon fibers, as shown in Figure 4.

Currently, PYROGRAF III production uses iron pentacarbonyl, natural gas and hydrogen sulfide as the sources of iron, carbon, and sulfur respectively. An economic scale-up analysis on the PYROGRAF III process performed by Battelle showed that the VGCF can be produced for under 5 \$/lb using the aforementioned feedstocks. Additional cost reduction would result from using coal fines as shown in Table 1. Reduction in the cost of the feedstocks is vital for allowing PYROGRAF III to be considered for automotive applications, such as in sheet molding compounds and numerous low strength components such as motor housings, interior panels, and other low-cost applications.

EXPERIMENTAL

A reactor used in PYROGRAF III production (Figure 1) was modified to allow the introduction of pulverized coal into the reactor. The reactor normally uses a feedstock mixture of natural gas, iron pentacarbonyl particles transported into the reactor by a helium stream, and 99.3% pure H_2S gas simultaneously injected into the 2000° F reactor. A typical control formulation that would produce a 25% yield is shown in Table 2. The apparatus to feed the coal fines is a Vibra Screw® Mini Feeder driven by a variable speed motor. The hopper is sealed to prevent the influx of oxygen which could cause immediate combustion of any fiber or hydrocarbons at the process temperature. The coal feeder transports the coal dust directly into the main gas feed to be carried into the reactor.

In the coal trials, the hypothesis is that sulfur-bearing coal can replace H_2S as the source of sulfur in the reaction. A combination of coal and methane were used as the hydrocarbon feedstock. The formulation was chosen such that the percentage of sulfur in the reactor derived exclusively from coal is equivalent to the "control" formulation of sulfur in the process when using methane only. Ohio #8 Coal from CONSOL Inc., at 4.71% total sulfur and 46.6% total carbon, was pulverized to less than 63 μ m. Methane was used as the carrier gas in Trial 1 at the rate required to balance the sulfur/carbon ratio to the control value. To determine the material balance, it was assumed that all the sulfur in the coal exists as hydrogen sulfide. In fact, the compounds of sulfur in coal vary extensively; however, as shown elsewhere⁷, the sulfur level can vary and still produce acceptable vapor grown carbon fiber.

RESULTS

Figure 5 is a micrograph of fiber produced from a mixture of coal and methane in which all of the sulfur was supplied by the coal. It is inferred from this micrograph that the sulfur contained in the coal plays an active role in the catalytic process, similar to the case where H_2S is used. The morphology of the fiber product and the absence of soot in this trial indicates comparable quality to the best material which can be produced by this method. Coal also contributes carbon to the process as can be inferred from Figure 6 in which fiber was produced using coal as the sole source of sulfur and carbon. In this micrograph the presence of soot is evident indicating that the sulfur to carbon ratio is unbalanced.

The degree of graphitic ordering is the crucial property that causes the wide range of strength and conductivity of carbon fibers. To estimate the degree of graphitization of the fiber produced with coal, X-Ray diffraction was used. Table 3 shows that the "as grown" samples using coal has graphitization in a range typical of a low modulus commercial fiber.

In the control process, which relies on H_2S introduced to a pure methane feedstock, periodic analysis has been made of the exhaust

emissions during trials. In the tests to date, sulfur has not been detected in the exhaust. During the present experimentation, the exhaust was sampled using gas chromatography, with a similar result. While the current GC analysis is relatively insensitive with respect to measurements on the control process, the detectability limit implies a sulfur concentration less than 1%.

Since the sulfur content in coal exceeds the control balance, such a result implies an optimistic consequence to a balanced sulfur content. These data taken together offer incontrovertable proof that VGCF can be generated from high sulfur coal. Furthermore, effort to optimize the formulation should result in carbon fiber generated from high sulfur coal with quality and efficiency comparable to processes using other hydrocarbon sources, and at costs enabling economic viability. Although further work is needed to assess the effects of the organics and ash content variation in coal, their presence does not prevent the growth of a carbon fiber with graphitic ordering, and would be acceptable in applications such as reinforcements for cement and rubber.

While these studies indicate the viability of using high sulfur coal as the hydrocarbon feedstock in the production of VGCF, in practice, the high percentage of sulfur in various coals, as well as the variability of the percentage of sulfur in coal, will most likely mandate a combination of hydrocarbon feedstocks in order to maintain the process balance needed for optimum production. The role of coal particulate in contributing both to the hydrocarbon balance and sulfur balance, is significant in any event.

CONCLUSIONS

It has been demonstrated that coal particulate can be used to produce VGCF, contributing both carbon and sulfur to the reaction. Work is in progress to optimize the process for conversion of coal fines to carbon fiber. Viability of the process will depend on the conversion efficiency, degree of graphitization of the fiber, percentage of ash in the product, and whether the process can be sustained on a continuous basis with an environmentally-benign exhaust. This work suggests an economical and ecologically safe process for the utilization of coal fines as the source material for carbon fiber reinforcements in rubber, cement, as well as composites for automobiles, electronics, and aerospace components.

ACKNOWLEDGEMENT

This research was supported in part by the U.S. Department of Energy under Grant No. DE-FG02-95ER81926. The authors also gratefully acknowledge the contribution Dr. David Anderson from the University of Dayton Research Institute in providing X-ray analysis.

REFERENCES

1. J.L. Kaae, Carbon **23**, 665 (1985).
2. G.G. Tibbetts, C.A. Bernardo, D.W. Gorkiewicz, and R.A. Alig, "Effect of Sulfur on the Production of Carbon Fibers in the Vapor Phase" CARBON, **32**, no. 4, pp.569-576, (1994).

Table 1. PYROGRAF III Material Cost Comparison

	High Purity Methane Only (\$/lb)	Natural Gas Only (\$/lb)	Coal Only @ \$30/ton (\$/lb)	Coal Fines Only @ \$23.50/ton (\$/lb)
Sulfur Source	0.189	0.194	0	0
Carbon Source	69.83	0.44	0.023	0.016

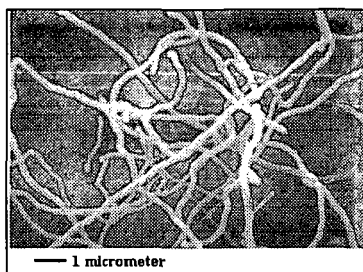


Figure 2. As-grown PYROGRAF III
Produced with Methane.

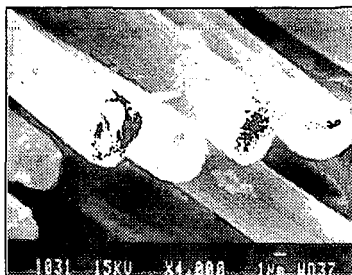


Figure 3. Commercial Carbon
Fiber.

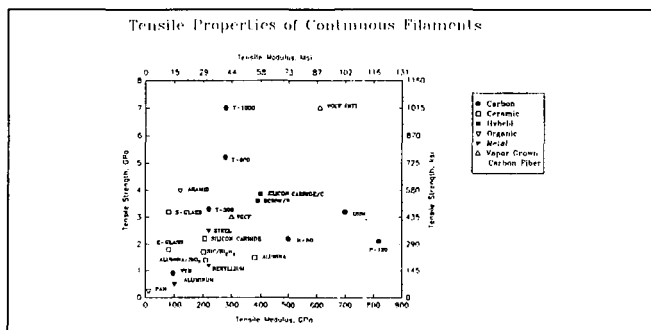


Figure 4. Tensile-Modulus Properties of VGCF.

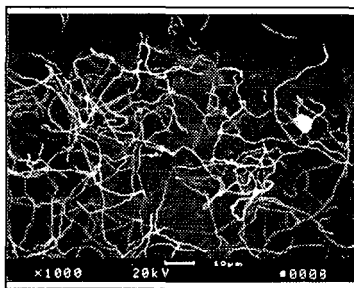


Figure 5. As-grown PYROGRAF III
Produced with Coal
Replacing H₂S.

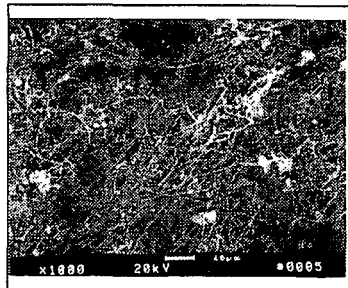


Figure 6. As-grown PYROGRAF III
Produced with Coal as
Sole Source of Carbon
and Sulfur

TABLE 2. Control Formulation for PYROGRAF III Production*

	CONTROL	TRIAL 1
Natural Gas	96.9	87.58
Coal	None	9.33
Sulfur	0.47	0.44
Helium	0.96	0.96
Fe(CO) ₅	1.68	1.69

* Formulations are in per cent by weight

Table 3. X-Ray Diffraction Analysis*

Heat Treat (C)	Fiber	D-spacing (nm)	g_p^* (%)
As-grown	VGCF	.34490	--
1300	ex-PAN	.354	--
As-grown	ATrial (coal)	.3459	--
2200	VGCF	.34206	23
2500	VGCF	.33770	73
2500	ex-PAN	.342	23
2700	VGCF	.33697	82
2800	VGCF	.33663	86
As-grown	PYROGRAF III	.3385	64
--	P-120	.3392	56
--	P-120	.3378	72

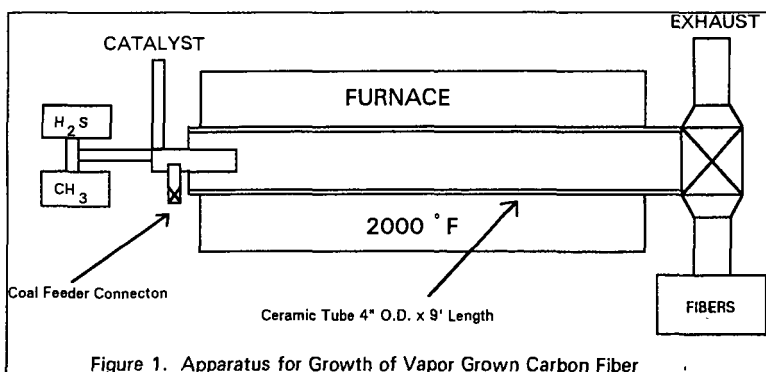
* $g_p = (.3440 - D\text{-spacing}) / (.3440 - .3354)$ 

Figure 1. Apparatus for Growth of Vapor Grown Carbon Fiber

MECHANICAL PROPERTIES OF CARBON FIBER COMPOSITES FOR ENVIRONMENTAL APPLICATIONS.

Rodney Andrews and Eric Grulke, Chemical and Materials Engineering Department, University of Kentucky, Lexington, KY 40506-0046.

Geoff Kimber, Center for Applied Energy Research, University of Kentucky, Lexington, KY 40511-8433.

Keywords: carbon fiber composite, activated carbon, mechanical properties, permeability

Abstract:

Activated carbon fiber composites show great promise as fixed-bed catalytic reactors for use in environmental applications such as flue gas clean-up and ground water decontamination. A novel manufacturing process produces low density composites from chopped carbon fibers and binders. These composites have high permeability, can be activated to have high surface area, and have many potential environmental applications. This paper reports the mechanical and flow properties of these low density composites. Three point flexural strength tests were used to measure composite yield strength and flexural moduli. Composites containing over 10 pph binder had an adequate yield strength of about 200 psi at activations up to 40% weight loss. The composites were anisotropic, having along-fiber to cross-fiber yield strength ratios between 1.2 and 2.0. The pressure drop of air through the composites correlated with the gas velocity, and showed a dependence on sample density.

Introduction:

The use of activated carbons for waste stream clean up is well known. However, the costs of using beds of adsorptive carbons are prohibitive in many cases. The uptake of chemicals into beds of granular carbon can be slow, and the pumping cost for beds of powdered carbons can be prohibitively high. The carbon fiber composites studied here have the advantages of high mass transfer rates inside the fibers, good mechanical strength, and high permeability to liquids and gases.

The composites were manufactured using a novel process developed at the University of Kentucky. ACFC's are made from amorphous carbon fibers which are "glued" together using a variety of binder systems. The binder works by cementing together fibers at their points of intersection. Binder may also adhere to the fiber surface, and can be activated as well.

These materials, which can be described as a highly porous solids, can be machined or formed to fit in many existing systems, and will act as fixed bed catalytic reactors for chemical removal or adsorption. Specific applications of these materials will result in different static and dynamic loadings. The composite parts must be able to withstand the loads seen during installation as well as operation and exhibit low pressure drop characteristics.

Mass Transfer Inside the Fibers

Reactants need to move from the bulk gas stream to the fiber surface, and then diffuse to reaction or sorption sites inside the fiber interior. One critical step in this sequence is the diffusion of the reactants inside the fibers. Because of the small diameter of the fiber, the rate at which this step takes place will be rapid compared to other factors in the process. The fibers have small pores through which gases and liquids can diffuse to the interior. The Fourier number for diffusion can be used with various unsteady state solutions to the cylindrical diffusion equation (Newman, 1931) in order to estimate the time needed to accomplish 90% of a step change in the gas phase concentration at the fiber surface. The diffusion coefficient of the solute is taken to be appropriate values for gas or liquid solutes, and the average fiber diameter was less than 25 microns. The Fourier numbers for the two types of carbons show that the diffusion time for a fiber is several orders of magnitude shorter than for a granular carbon particle (Table 1). The fibers used in the ACFC's studied here have intrinsically rapid uptake rates for both gas and liquid systems.

Mechanical Strength

The activated carbon fiber composites would be used either as flat filters treating the entire gas flow, or as annular (candle) filters arranged in a bag house type system. In either case, the filter unit would require good flexural strength. It also must withstand installation, cyclic loading, and, for some applications, regeneration. These criteria have led us to evaluate the mechanical performance of the composites using flexural tests. In addition, some applications will require complex composite shapes which are expected to be anisotropic due to the nature of the forming operation. Therefore, measurements in the machine and transverse directions are compared.

Permeability to Gases and Liquids

Activated carbon fiber composites (ACFCs) can be used in gas phase processes because of their low pressure drops and high internal mass transfer rates. Possible uses include low temperature removal of sulfur dioxide and nitrogen oxides from flue gas streams. The flue gas velocities are on the order of 3 meters per second, requiring high reaction rates, high mass transfer rates, and low pressure drop operation for economic treatment. The pressure drop for a fluid flowing through the composite can be compared to that of a fluid in a packed bed. The commonly used model for flow in a packed bed is the Ergun equation:

$$\frac{\Delta P}{L} = \frac{150\mu U}{D_p^2} \cdot \frac{(1-\epsilon)^2}{\epsilon^3} + \frac{1.75\rho U^2}{D_p} \cdot \frac{1-\epsilon}{\epsilon^3}$$

where ($\Delta P/L$) is pressure drop per length, U is the superficial velocity, D_p is the effective fiber diameter, μ is the fluid viscosity, ρ is the fluid density, and ϵ is the composite void fraction. As the system studied does not follow the

assumptions necessary for use of the Ergun equation, a modified form of the equation was used in this study. This is equation is

$$\frac{\Delta P}{L} = K \cdot (U^*)^n,$$

with K being a parameter dependent on the fluid properties, and n is between one and two. U^* , the corrected velocity, is defined by

$$U^* = \frac{(1 - \varepsilon)^2}{\varepsilon^3} \cdot U.$$

Objectives

This study measures the failure strength and the permeability of a novel activated carbon fiber composite. The mechanical properties of these materials were studied using modified ASTM flexural testing methods. Pressure drop was correlated with gas velocity and the density of the composite.

Experimental:

The composites were tested to determine flexural strength at break, maximum strain, and the elastic modulus of the material. Samples were formed in 4 inch diameter cylinders, about 4 inches in height. ASTM standard C203-92 (3 point bend flexural testing of block type insulation) was followed. The samples were cut from the block in two directions. The cross direction is the plane parallel to the direction of composite formation. The along direction is the plane perpendicular to the direction of formation. The samples were tested using a three point apparatus on an Instron.

Scanning electron micrographs were taken of the fracture plane of the samples. SEM analyses were used to identify failure mechanisms and binder distribution in the samples. In most cases, the samples were sputtered with gold and then analyzed at 600x magnification.

Pressure drop measurements were made using an Omega DP41-E High Performance Process Indicator and 0 - 2 psi microtransducer. Nitrogen at controlled volumetric rates was passed through composite samples until a constant pressure drop was determined for each flow rate.

The variables effecting the flexural strength of the composites were: fiber length, binder content, thermal treatments, and preactivation of the fibers before formation. The binder used in composite formation is a phenolic thermoset. All fibers used were obtained from Ashland Chemical and have an average diameter of 17 microns. Samples were made which contained differing binder quantities: 5, 10, 20 and 40 parts per hundred. Each of these samples were also tested under all of the activation phases: cured, baked, and activated at 10%, 20% and 40% weight loss.

Several different thermal treatments were studied: curing, baking, and activation. During curing, the composite is held at 150 °C to completely cure the binder resin. The composite is baked in an inert atmosphere at > 650 °C. Activation is done by heating the composite at temperatures greater than 750 °C in a carbon dioxide or steam atmosphere.

Results:

Composite Morphology

The 5 pph binder composites were found to be too weak for practical application, and friable during handling for all thermal treatments. Because of this poor sample integrity, the 5 pph samples were difficult to test, and had low reproducibility. SEM analysis of these composites showed binder wicking at the fiber contact points during the curing process. Some of the fiber contact points were not wetted with binder, and the fiber surfaces were not been coated with binder.

The 10 pph binder composites exhibited much higher strength than the 5 pph samples. In the SEM analysis of the 10 pph binder composites, most of the fiber contact points are wetted with binder. Some of the excess binder wicks onto the fibers, completely covering the fibers in samples containing 20 pph binder. This wicking of binder to cover the fibers continues at the 40 pph binder content level and gives a thick coating.

Mechanical Strength

The flexural strength at break of standard samples made with P400 fibers and cured only were compared in the cross- and along-fiber directions. These samples were found to exhibit anisotropy. The yield strengths of these samples are adequate in all samples except the 5 pph binder content sample. The yield strength increases with increasing binder weight fraction. The level of anisotropy is 1.1 to 2.0 based on cross- to along-fiber strengths. (Figure 1).

More thermal processing reduces yield strength and elastic modulus. This trend is true for samples with differing binder contents as well (Figure 2). The effect of thermal processing can also be seen in the SEM analysis. Composite samples containing 40 pph binder before curing were activated to 13, 19, and 35 % weight loss. At 13%, binder completely coats the fibers. At 19%, binder still coats the fibers, although not as thickly. At 35 % weight loss activation the fibers are no longer coated with binder. At each activation level, evidence of binder failure, fiber pullout, and flaking of the binder away from the fibers can be seen. This indicates a failure mechanism of fiber pullout, or, failure of the fiber binder interface.

Fiber length has a significant effect on composite strength. The shortest fibers, P200's with a length of 350 microns, result in the composite with the highest flexural strength at break. The longest fiber, at 10,000 microns, has the longest span between binder contact points, resulting in the weakest composite. See Table 2.

Composite mechanical properties decrease with increasing thermal processing. Cured composites are the strongest, have the highest modulus, and have the highest density. Baked samples have a lower density, but also have lower strength and modulus. Activated samples have the lowest strength, the lowest modulus, and the lowest density (Table 3). This could be a result of the binder coating acting to stiffen the fiber-binder piece. At higher stages of thermal processing, excess binder is burned away, and the strength of the composites decrease. This trend of decreasing modulus and strength with increasing thermal processing is seen in composites made from medium and long fibers as well.

Higher amounts of binder in the composite make it stronger, but increase the density. Normalized moduli (E/ρ) increase directly with binder content, suggesting that the binder contributes directly to material strength (Table 4).

Composite Flow Characteristics

Pressure drop per unit length increases with composite density, and with increasing fluid superficial velocity (Figure 3). The data is fitted by the modified Ergun equation: K equals 288 for nitrogen and n is 1.168 (Figure 4). Ninety-eight percent of the data fall within two standard deviations of this fit. Thermal processing has no significant effect on pressure drop. The composites are isotropic with respect to pressure drop.

Conclusions:

Variables which effect the strength and modulus of activated carbon fiber composites are fiber length, binder content, and level of thermal processing. The composites show strength anisotropy, 1.1 to 2.0, between the cross- and along-fiber alignment directions.

SEM micrographs show that the failure mechanism for these composites is fiber pullout. Increasing binder content leads to thicker layers of wicked binder coating the fibers. Thermal processing burns away the binder, resulting in a weaker composite with lower density.

For most applications, the strength of composites with 10 parts per hundred binder and higher composites would have adequate strength for low pressure drop systems at activations up to 40% weight loss. This implies great flexibility in application and tailoring of the composite morphology for different catalytic systems.

The effect of fiber length was as expected. Composites made with shorter fibers have higher densities, higher yield strengths at break, higher elastic moduli, and a lower elongation at break. Thermal processing reduces the composite strength and moduli because the wicked binder is burned away.

The composite is highly permeable to gas flows, and has a low pressure drop at industrial flue gas velocities. The pressure drop in the composites can be accurately predicted using a modified form of the Ergun equation. Pressure drop is proportional to the corrected velocity to the 1.168 power, and K , the proportionality constant, is 288 for nitrogen.

Table 1: Time to accomplish 90% of a step change in the surface concentration.

Carbon Form	Length Scale, cm	Gas Phase (90%), s	Liquid Phase (90%), s
fiber	0.0025	0.000005	0.05
granule	0.10	0.032	320

Table 2: Effect of fiber length on strength.

Fiber	Length, microns	Strength, psi
P200	350	324
P400	700	215
P3200	10,000	8.5

Table 3: Effects of thermal processing on short (P200) fiber composites.

Thermal Stage	Dry Density, g/cc	Strength, psi	Modulus, psi
cured	0.330	324	39,000
baked	0.309	249	14,200
activated	0.261	157	9,870

Table 4: Effect of binder content on normalized modulus. P400 fibers.

Binder Content, part per hundred	Modulus, psi	Dry Density, g/cc	E/p
10	6,430	0.210	30,600
20	10,300	0.220	46,800
40	22,000	0.237	92,800

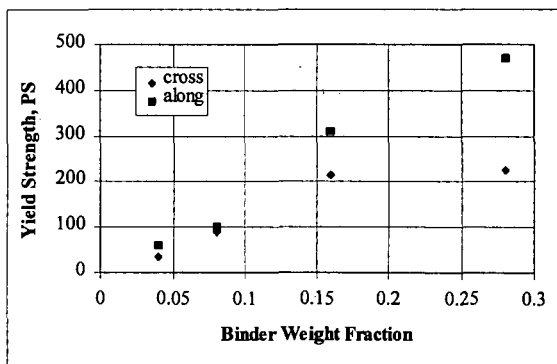


Figure 1. Effect of binder weight fraction on Yield Strength. P400 fibers, cured.

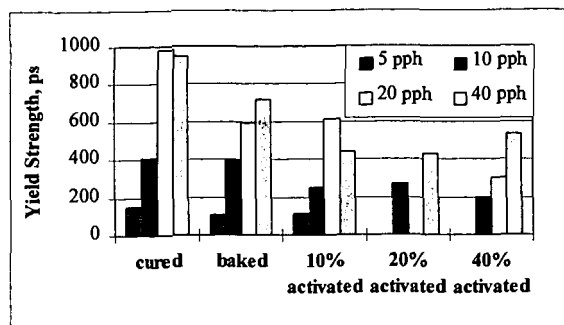


Figure 2. Yield strength over the processing lifecycle.

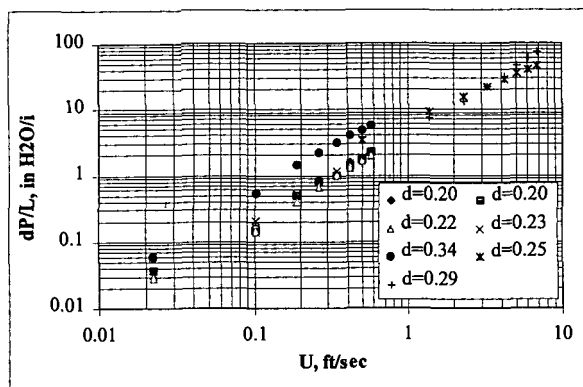


Figure 3. Pressure Drop versus Superficial Velocity.

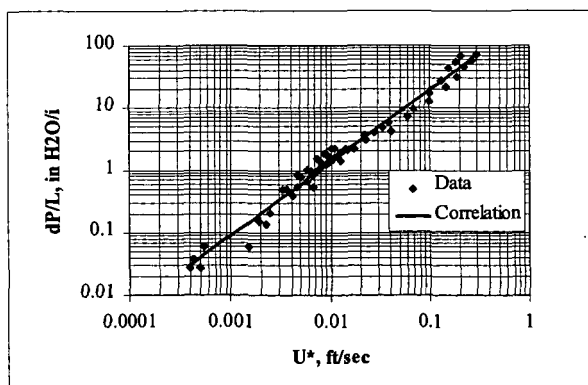


Figure 4. Pressure drop versus corrected velocity. $K = 288$, $n = 1.168$.